BASIC INTEGRATIVE MODELS FOR OFFSHORE WIND TURBINE SYSTEMS

A Thesis

by

FARES ALJEERAN

Submitted to the Office of Graduate Studies of
Texas A&M University
in partial fulfillment of the requirements for the degree of

DOCTOR OF PHILOSOPHY

May 2011

Major Subject: Ocean Engineering

BASIC INTEGRATIVE MODELS FOR OFFSHORE WIND TURBINE SYSTEMS

A Thesis

by

FARES ALJEERAN

Submitted to the Office of Graduate Studies of
Texas A&M University
in partial fulfillment of the requirements for the degree of

DOCTOR OF PHILOSOPHY

Approved by:

Chair of Committee,	John M. Niedzwecki
Committee Members,	Billy Edge
	Charles Aubeny
	H. Joseph Newton
Head of Department,	John M. Niedzwecki

May 2011

Major Subject: Ocean Engineering

ABSTRACT

Basic Integrative Models for Offshore Wind Turbine Systems. (May 2011)

Fares Aljeeran, B.S., Kuwait University;

M.S., Texas A&M University

Chair of Advisory Committee: Dr. John M. Niedzwecki

This research study developed basic dynamic models that can be used to accurately predict the response behavior of a near-shore wind turbine structure with monopile, suction caisson, or gravity-based foundation systems. The marine soil conditions were modeled using apparent fixity level, Randolph elastic continuum, and modified cone models. The offshore wind turbine structures were developed using a finite element formulation. A two-bladed 3.0 megawatt (MW) and a three-bladed 1.5 MW capacity wind turbine were studied using a variety of design load, and soil conditions scenarios. Aerodynamic thrust loads were estimated using the FAST Software developed by the U.S Department of Energy's National Renewable Energy Laboratory (NREL). Hydrodynamic loads were estimated using Morison's equation and the more recent Faltinsen Newman Vinje (FNV) theory. This research study addressed two of the important design constraints, specifically, the angle of the support structure at seafloor and the horizontal displacement at the hub elevation during dynamic loading. The simulation results show that the modified cone model is stiffer than the apparent fixity level and Randolph elastic continuum models. The effect of the blade pitch failure on the offshore wind turbine structure decreases with increasing water depth, but increases with increasing hub height of the offshore wind turbine structure.

ACKNOWLEDGMENTS

I would like to use this opportunity to thank my supervisor, Prof. John M. Niedzwecki, for his constant support. I also thank my supervisory committee for their dedication and concern and special thanks to Prof. Jose M. Roesset for his support.

TABLE OF CONTENTS

Page

Page

LIST OF FIGURES

FIGURE Page

FIGURE Page

LIST OF TABLES

1. INTRODUCTION

Energy is at the core of global economics and reaches down into everyday life. Energy can be categorized as being derived from either renewable or non-renewable sources. Renewable green energy sources, sometimes referred to as green energy sources, include energy derived from wind, hydrokinetic, geothermal, and biomass. In contrast, non-renewable sources of energy include hydrocarbon (oil & gas) and coal. Consumption of nonrenewable energy is increasing rapidly as the world's population continues to grow, and there is great concern about the prospect of its depletion and the pollutants produced as a byproduct of its consumption. From an environmental perspective, nonrenewable energy sources continue to contribute significantly to pollution of the atmosphere through CO_2 production and are considered to be the major force driving global warming.

In an effort to address these problems, many countries have been aggressively targeting goals for inclusion of renewable energy sources to be consequently, a major component of their future energy consumption. Because of its potential globally, wind power is receiving more attention than any other source of renewable energy because wind farms can be located on land or off the coast at offshore sites and much of the onshore technology is proven and available. Energy derived from the conversion of wind creates almost no pollution, although closeness to population center intermittency and storage of energy are topics for current research. Because of its intermittent nature it is seen to be a complementary energy source to more conventional sources of electrical energy. Most analysts expect that this technology sector will grow very rapidly especially

---

The dissertation follows the style and format of Ocean Engineering.

offshore in the near future.

The basic concept of wind power technology is to deploy a device that converts wind speed directly into usable electricity that could be used immediately on the grid or perhaps be stored for later use. The blades on a wind turbine rotate about a hub and harvest the wind's kinetic energy by turning an electric generator via a drive shaft and gearbox. Using wind energy technology, an individual home or small business can potentially generate sufficient electricity for its needs through use of a single wind turbine rated between 2.5 kW to 12 kW. Further, "wind farms" that are comprised of a number of wind turbines can be used to power private or commercial enterprises. The potential to create more energy for consumption from wind farms sited at locations near population centers is a critical issue for the public and investors. This dissertation research will focus on the engineering aspects of modeling the dynamic response behavior of fixed wind turbine tower and foundation design for near-shore coastal regions.

Recently, the number of offshore wind farms that have been built, the number of units that have been installed for offshore wind farms, and the total power of offshore wind farms that have been built have been rapidly increasing, as demonstrated in Fig. 1, Fig. 2., and Fig. 3. The data shows the recent trend towards more offshore wind farm development and towards larger wind farms. There are important advantages for locating wind farms at offshore sites as there are higher wind speeds (see Fig. 4) and the potential for more constant wind speed than at onshore sites. In addition, offshore sites can be selected to minimize the visual and noise pollution that generally accompanies land-based sitting of wind farms, and the use of offshore sites provides for the possibility of

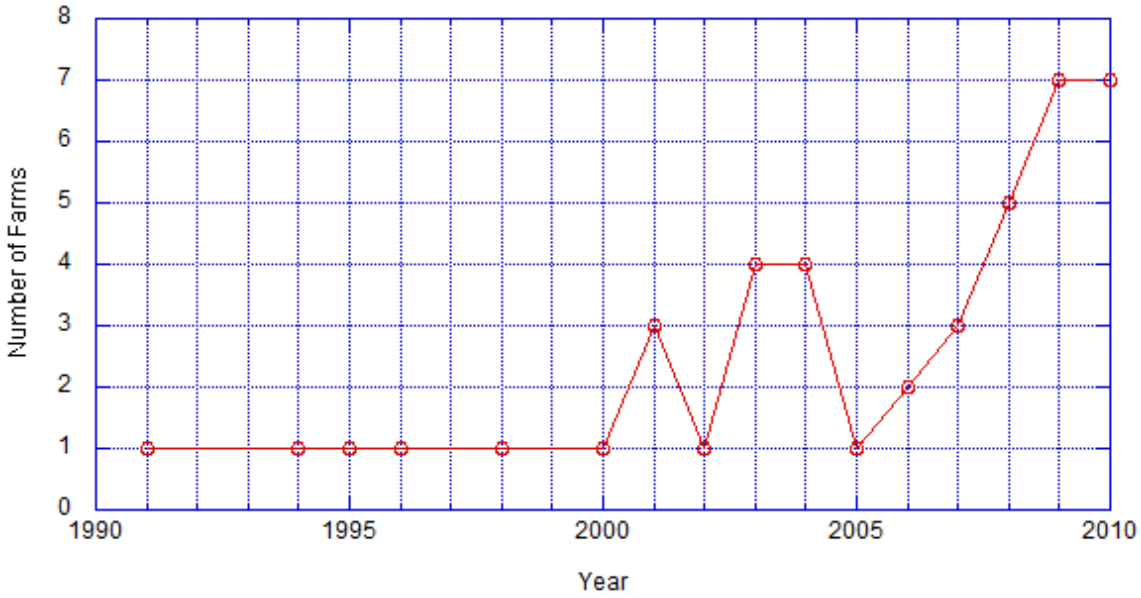

Fig. 1. The Number of Offshore Wind Farms that Have Been Built Worldwide Since 1991 (Appendix-A)

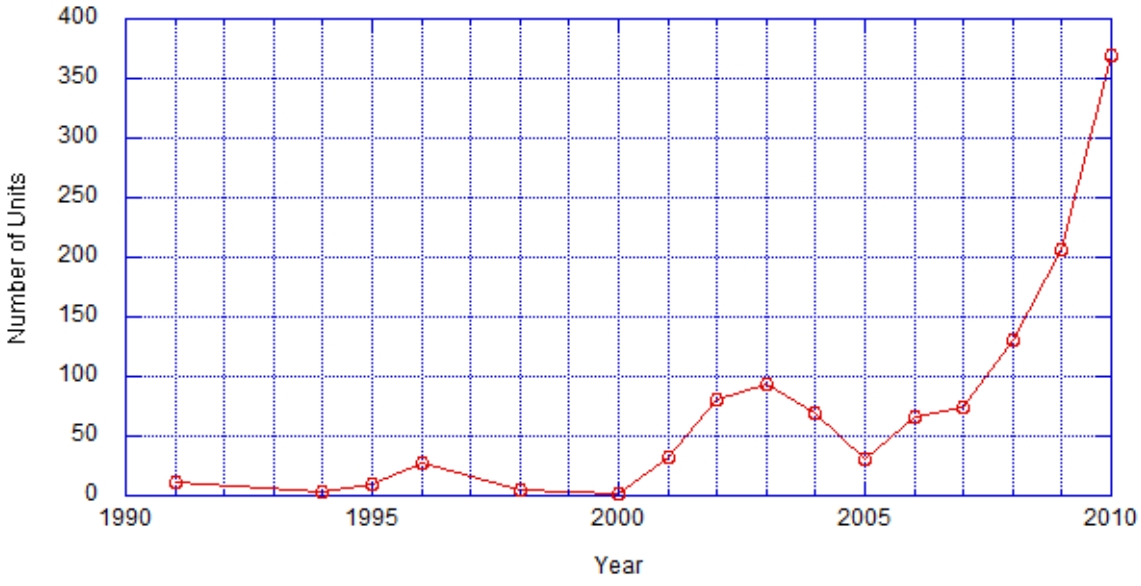

Fig. 2. The Number of Units that Have Been Installed for Offshore Wind Farms Worldwide Since 1991 (Appendix-A)

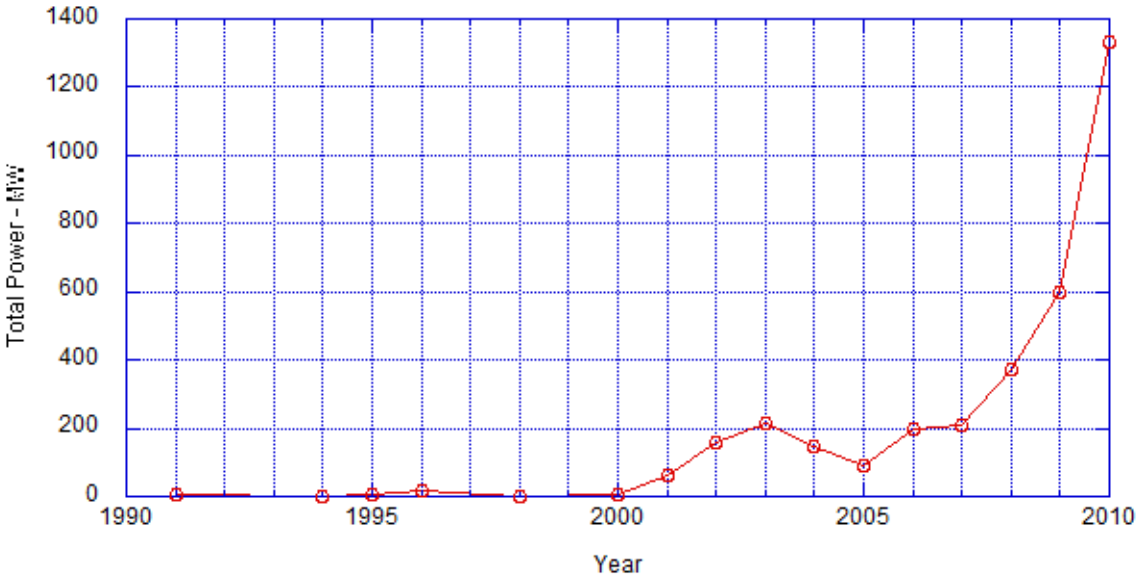

Fig. 3. The Total Power of Offshore Wind Farms that Have Been Built Worldwide Since 1991 (Appendix-A)

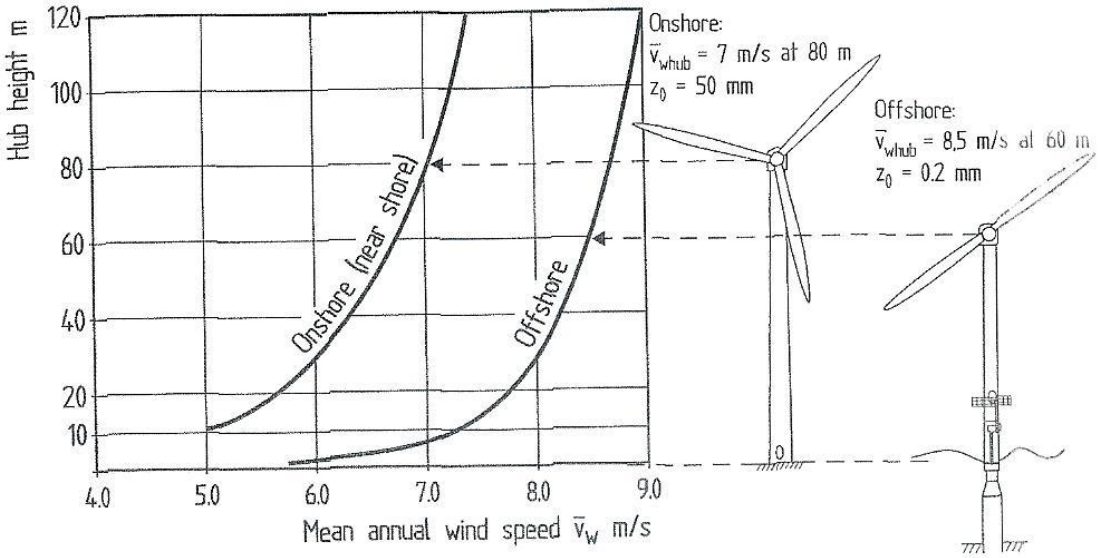

Fig. 4. A Generic Comparison of the Mean Annual Wind Speed Profiles for Onshore and Offshore Location as Related to the Hub Elevation of a Wind Turbine (Hau 2005)

installing larger wind farms. A major concern when developing offshore wind farms is the cost of the foundations, which can be on the order of 25% to 35% of the total cost (Byrne & Houlsby, 2003). It is therefore important to consider a variety of options when selecting the foundation type (gravity-based foundation, monopile foundation, or suction caisson foundation) as an integral part design of individual tower systems as the dynamic response behavior of each tower can vary within the wind farm. Thus, an integration model allowing for these type of modeling issues will be developed.

1.1 Wind Energy Resource

One of the first steps to constructing a wind farm is to evaluate the wind resource areas and estimate the wind energy in those areas. It is crucial that any wind energy project obtain a correct estimation; otherwise, the entire project may fail. In September 2010, the U.S. Department of Energy's (DOE) National Renewable Energy Laboratory (NREL) reported the wind resource in the 48 contiguous states, except for Alabama, Florida, and Mississippi (see Fig. 5). The wind resource map shows the land-based and offshore wind resources at 50 m above the surface. Apparently, the map reveals a significant advantage in the offshore wind area over the land-based wind area, which means that the development wind projects will focus more on the offshore areas. However, challenges may occur regarding regulations, site restrictions, and public concerns. Until now, all wind energy projects in the United States are land-based projects; no offshore wind energy projects exist to date. The mapping status of the in-progress, planned, and future offshore projects are shown in Fig. 6. The NREL estimates that the United States could feasibly build 54 GW of offshore wind power by 2030, which means 20% of its electricity will come from wind power. One way to achieve this

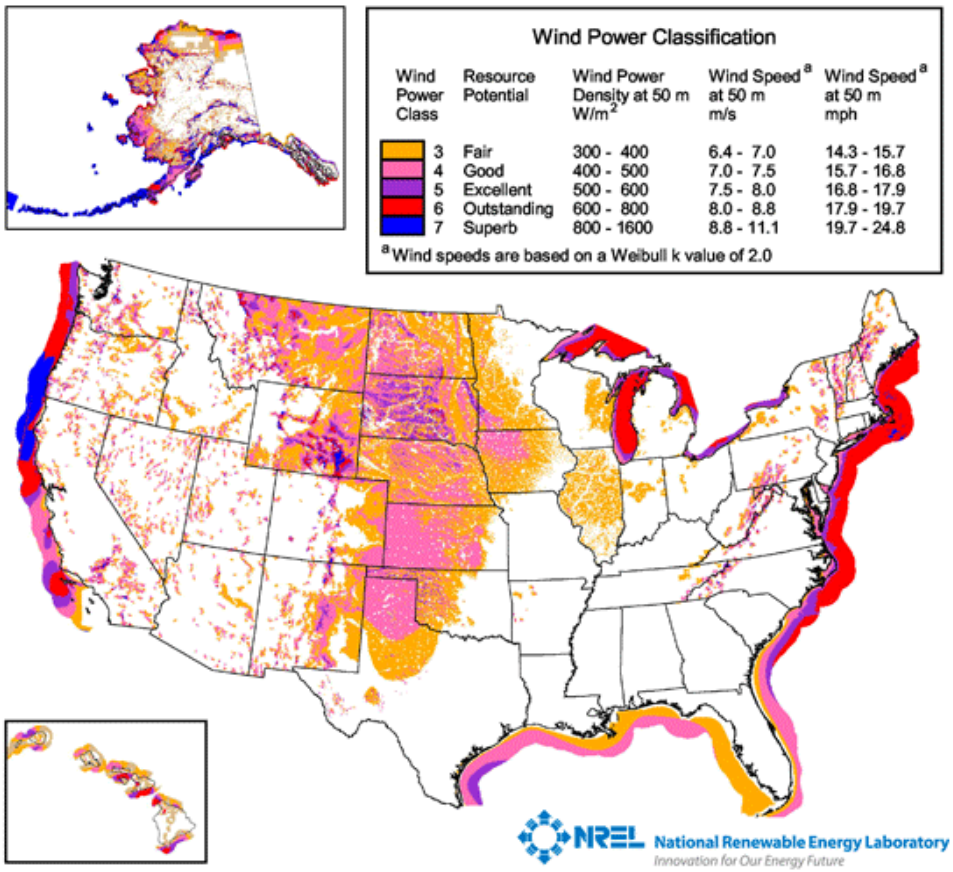

Fig. 5. The Annual Average Wind Power Estimates at 50 m Above the Surface (Musial and Ram 2010)

Fig. 6. The in Progress, Planned, and Future Offshore Projects in the U.S. (Elliott and Schwartz 2006)

goal is by developing more offshore wind energy projects in the near future.

Europe started the first offshore wind farm in 1991 and has held the lead since then in offshore wind power capacity. European Environment Agency (EEA) presents a map that shows the land-based and offshore wind resources (see Fig. 7). From the map, it can be seen that the average wind velocity offshore is higher than the land-based average wind velocity, which means there is more wind energy power offshore than onshore. More offshore wind projects have been built since 1991, and Fig. 8 depicts the operational offshore wind farms in Europe until 2009. The European Wind Energy Association (EWEA) has reported that the estimation of the wind energy by 2030 will cover between 21% and 28% of Europe electricity demand, and half of it will come from the offshore wind power projects.

1.2 Literature Review

There are many factors that should be taken into consideration when selecting a turbine size, such as site regulation, location, the budget, plan and maintenance requirements. Site regulations vary according to country and locality and in general, these regulations limit the location, height, and other characteristics of the turbine. Location and elevation play an especially important role in determining the potential energy available, based upon annual wind speed measurements. On the average, wind speed increases with hub elevation as was illustrated in Fig. 4. According to Gipe (2004), at a site with a temperature of 15^{o}C (59^{o}F) with a corresponding air density of 1.225 kg/m^3 the annual power density (power/swept area) in kW/m^2 can be estimated using the following equation:

$$P / A = 0.6125 \times 10^{-3} \times (V)^3 \times 1.91 \quad (1)$$

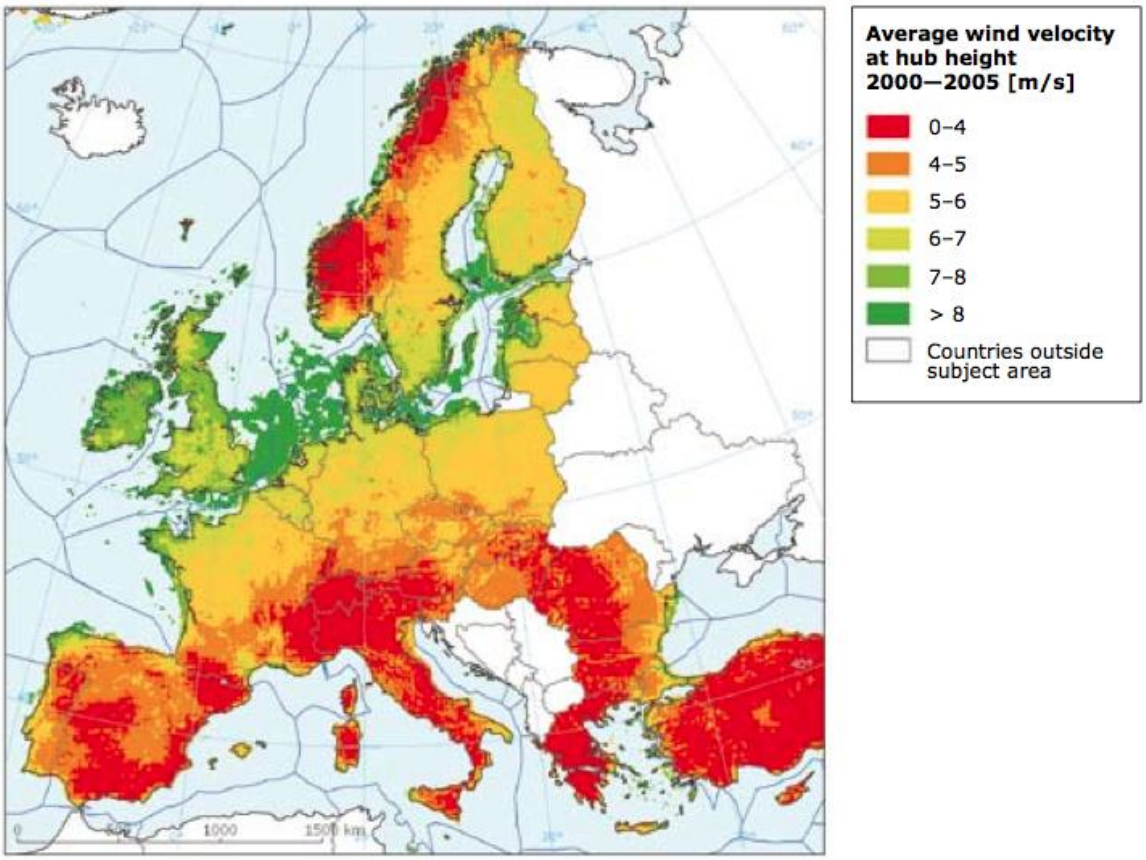

Fig. 7. Europe Land-Based and Offshore Wind Resources in 2008 (EEA)

Fig. 8. Operational Offshore Wind Farms in 2009 (http://www.ewea.org)

where V is the mean wind velocity. The annual energy output (AEO) in kWh/yr for single wind turbine can be estimated based upon area swept by the turbine blades and the efficiency of the wind turbine, using the following equation:

$$AEO = P / A \times A \times (\%efficiency) \times 8,760 \times 1,000 \quad (2)$$

The focus for this research investigation will be limited to horizontal axis wind turbines whose rotor assembly involves two or three horizontally rotating blades. Three-blade type wind turbine designs are more efficient, and are reported to run more smoothly than the two-blade version systems (Gipe 2004). Also the three-blade wind turbine generates more thrust force on the rotor than the two-blade rotor. Wind turbine blades are made from a variety of materials including fiberglass composites or wood, and must be lightweight, strong, and flexible. Turbine efficiency is one of the key factors that can increase the annual energy output of the wind turbine, but will only be considered as a parameter to be varied in this research study, as the energy output from a wind turbine is more sensitive to wind speed and swept area. According to Gape (2004), the theoretical maximum limit of the power efficiency of the rotor is 59.3%, also known as the Betz limit after Albert Betz the German aerodynamicist. In general, wind turbines can capture between 12% and 40% of the annual energy contained in the wind, depending on the location and type of wind turbine. Wind turbine towers vary in design, as shown in Fig. 9.

The American Wind Energy Association (AWEA) states that onshore wind turbine blades clearance needs to be at least 9.1 m (30 ft) higher than any other structures, trees, or bluffs within 91.44 m (300 ft) of the wind turbine tower in order to minimize the effects of turbulent flow. This is illustrated in Fig. 10. Wind farms incorporating more than one wind turbine must also take wake effects, which can decrease efficiency. Wake

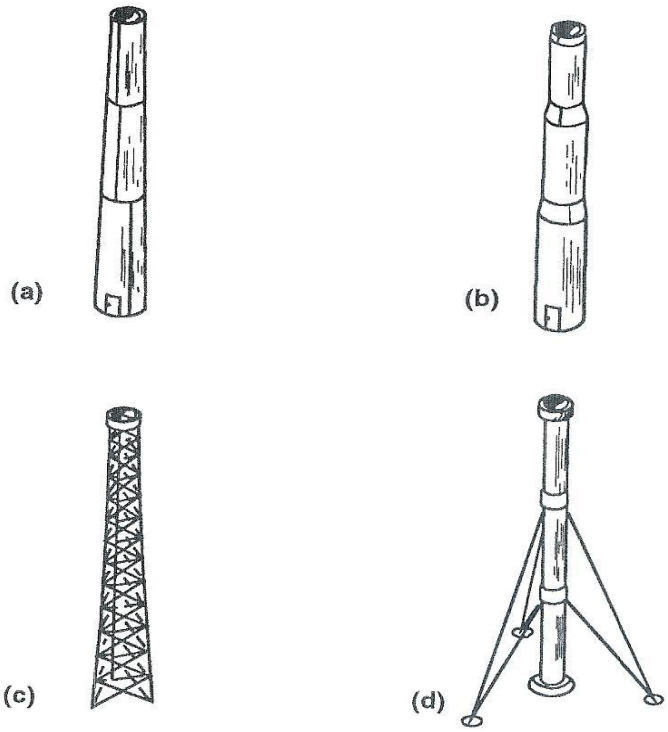

Fig. 9. Typical Horizontal-Axis Wind Turbine Tower Designs: a) Shell, b) Stepped Shell, c) Truss (or Lattice), and d) Guyed Shell (Spera, 1994)

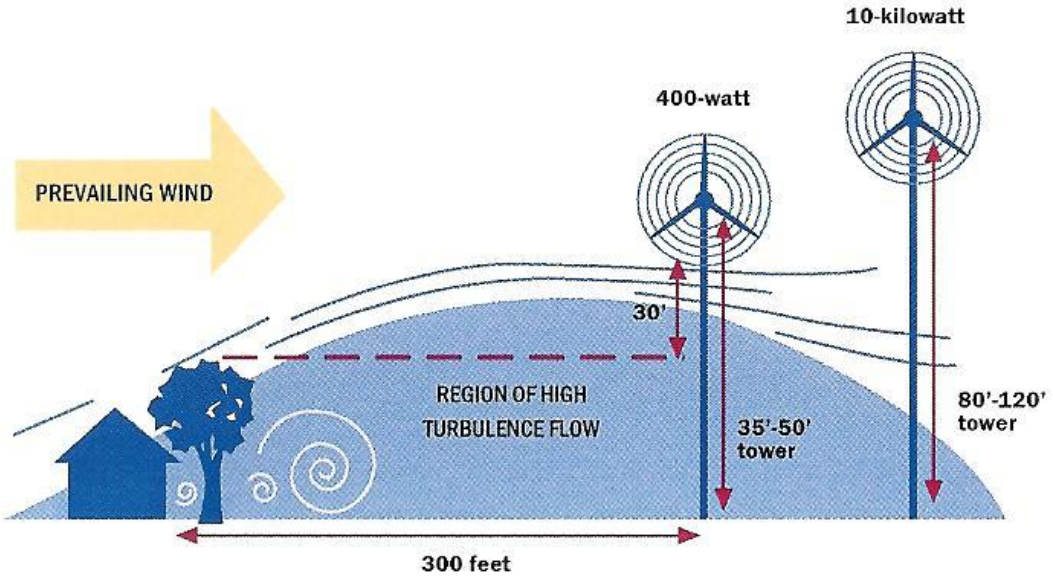

Fig. 10. Example of Suggested Tower Hub Elevations for Single-Home Wind Turbines (American Wind Energy Association, 2003)

effects can be minimized through careful spacing of individual turbines (IEC 61400-1, 2005). According to (Hau, 2005), the wake area can be divided into three regions, namely the near wake, intermediate or transition, and far wake regions. The near wake region includes the area behind the rotor between one to two rotor diameters (1-2D). The intermediate region, which covers the distance beyond the near wake region between two to four rotor diameters (2-4D). Finally, The area behind the rotor at five or more rotor diameters (5^{+}D) is termed the far wake region, which is the region often assumed to be best suited for positioning the next rotor, as it contains the least deceleration of wind velocity. The Danish Wind Industry Association (DWIA) recommends that the distance between towers be between five and nine rotor diameters (5-9D) in the dominant wind direction and between three and five rotor diameters (3-5D) at a 90-degree angle to the dominant wind direction. The Tunø Knob wind farm has two rows of five Vestas 500 kW wind turbines with a spacing of 5.1 rotor diameters perpendicular to the dominant wind direction and 10.2 rotor diameters in the dominant wind direction (Ferguson et al. 1998). For Vindeby wind farm, two lines of five and six Bonus 450 kW wind turbines are spaced at 8.6 rotor diameters in both directions. Nevertheless, it is important to take into account that rotor diameters vary considerably within the wide range of wind turbine equipment available. For instance, the very small Marlec 500 has a rotor diameter of 0.5 m (1.7 ft), while the enormous Vestas 90-model has a rotor diameter of 90 m (295 ft) (Gipe 2004). The difference in potential electrical power these two models can produce is substantial, with the Marlec 500 capable of producing approximately 20 W of electrical power comparing to the V90, which can produce up to 3 MW.

Other critical design variables include tower height, tower material (steel, concrete, or

wood), rotor blade type shape, and soil conditions of the foundation. Since foundations represent about 25% to 35% of the cost of wind farm installation, selecting between pile, suction caisson, and gravity-type systems becomes an important design consideration. The selection depends upon soil characteristics, such as strength and stability. The variety of foundation types available for near-shore wind tower structures are pictures in Fig. 11. Approximate dimensions have been applied to Fig. 11 in order to provide a visual representation of just how large a 3MW offshore wind turbine can be. Foundation types are expected to vary depending upon the location of the wind farm. For example, according to (Byrne & Houlsby 2003), a gravity-based foundation type [see Fig. 11 (a)] was used at the Middelgrunden and Nysted Havmollepark wind farms in the Baltic Sea. Horns Rev, located in the North Sea 14 kilometers west of Denmark utilizes a monopile foundation type [see Fig. 11 (b)] while a trial suction caisson foundation type [see Fig. 11 (c)] has been constructed at Frederikhavn in Denmark. The suction caisson foundation is particularly interesting due to its potential relative ease of installation and removal.

An offshore wind turbine structure (OWTS) can be viewed as consisting of three major system components the upper section (the rotor assembly with blades), the middle section (the tower), and the lower section (the transition piece and the foundation). Offshore environmental design loads may involve a combination of wind, wave, and currents varies, depending upon the particular location of the offshore site. A design storm with a 50-year return period has been deemed appropriate for offshore wind turbine structures by the US Army Corps of Engineers. In the design process tower strength, tower stability, resonant frequencies, and fatigue loading are important design aspects. In particular, care must be taken that neither the rotor frequency (f_r) nor the blade passing

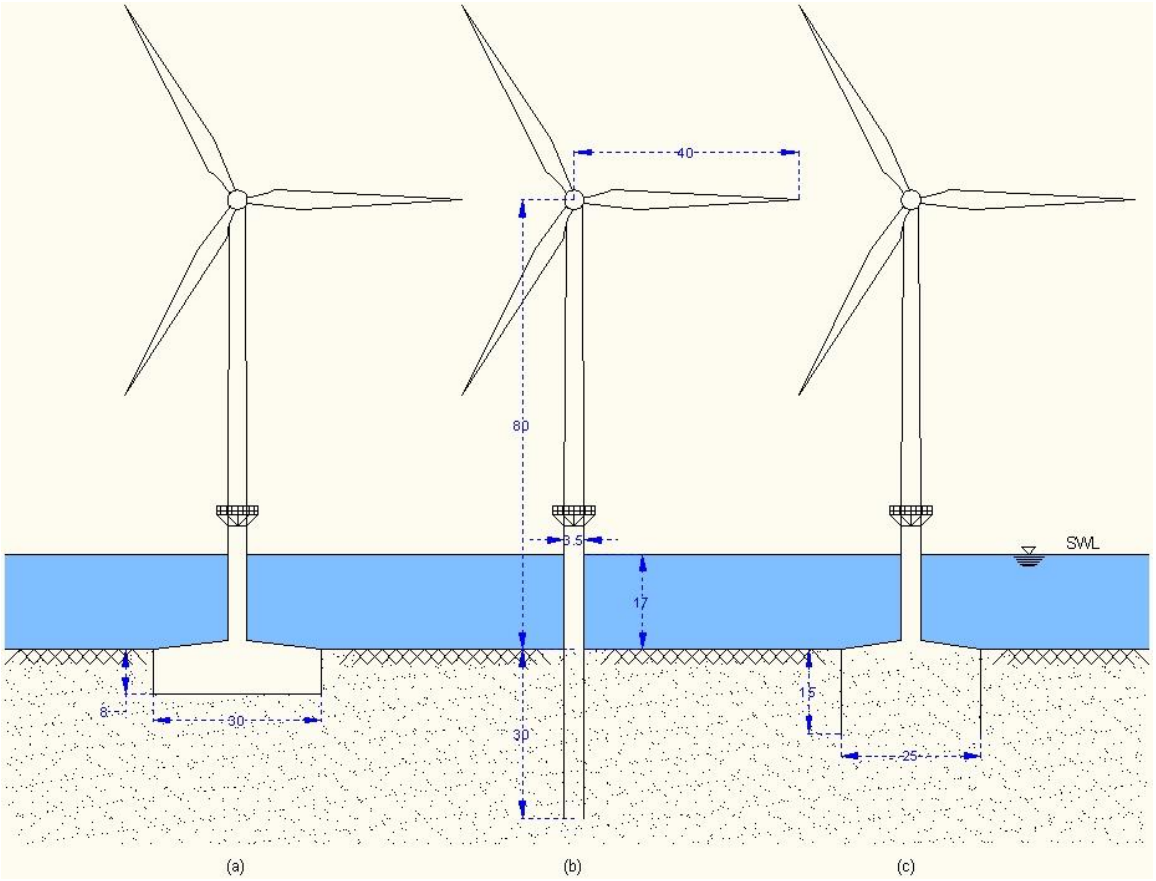

Fig. 11. Foundation Types for Near-Shore Wind Tower: a) Gravity-Based, b) Monopile, and c) Suction Caisson

frequency (f_b) match the fundamental natural frequency (f_o) of the overall wind turbine structure. Three different design solutions are possible for offshore wind turbine structures, depending on the ratio between f_o, f_r, and f_b. These include stiff-stiff design, if $(f_b < f_o)$, soft-stiff design if $(f_r < f_o < f_b)$, and soft-soft design if $(f_o < f_r)$. Overtime an important factor that can reduce the fundamental natural frequency (f_o) is the presence of marine growth on the subsea support structure. It presence will increase the structure's mass without noticeably affecting structural stiffness. Soft fouling and hard fouling organisms make up the two kinds of marine growth as discussed by Hallam et al. (1978) and they suggest using the data presented in Table 1 to estimate the mass of marine growth if no other information is available. Scour of the seabed around the subsea structure can reduce the fundamental natural frequency of an offshore wind turbine structure. This is particularly a concern for monopile foundations in region of sandy seabeds as scour changes the embedment depth. Engineering solutions to this problem include: 1.) preventing the scour from happening by adding layers of asphalts, concrete mattresses, or crushed rocks on top of the seabed, or 2.) anticipating the depth of the seafloor scour and accounting for this in the analysis, so that the range of the fundamental natural frequency of the structure does not overlap (thereby avoiding resonance phenomena) with the rotor frequency, the blade passing frequency, or the range of wave frequencies.

1.3 Some Innovative Wind Turbine Developments

In this section, we will address some interesting information regarding wind turbine innovations as well as the latest updates and developments in onshore and offshore wind turbine technologies. Wind technology can be utilized to power highways, as Ariel

Table 1 The Mass of Marine Growth per Surface Area of Different Ranges of Depths (Hallam et al. 1978)

Depth below mean water level	Mass per surface area (kg/m^2)
0-10	250
10-20	200
20-30	125
30-50	80
Over 50	<20

Schwartz discusses on inhabitat.com (see Fig. 12). Although it is still in the conceptual phase, the idea is to use the moving air from passing highway vehicles to generate more wind, thus increasing the wind speed around wind-powered highway lights. Nevertheless, a certain degree of uncertainty exists regarding the extent of power that can be generated from vehicles passing by wind-powered highway lights. Meanwhile, businessweek.com reports that FloDesign Wind Turbine has developed a prototype model based on features taken from the jet engine design (see Fig. 13). This wind turbine model will be three times as efficient as the typical three-bladed model, as Stanley Kowalski III, CEO of FloDesign Wind Turbine, claims. The new model incorporates a combination of small blades with special vents set up to create spinning vortexes as air passes through the vent slots. The main advantages of this model over the conventional model include smaller wind turbines, greater efficiency, and reduction in transportation costs. Ransom and Moore (2009) published an article exploring an alternative wind turbine concept that makes use of an array of small wind turbines. The idea was to replace a single turbine of 200-meter diameter with 20 turbines, each of which possesses a diameter of 45 meters. With respect to the swept area, both designs are (theoretically) virtually identical in terms of power production. In order to prove this theory, a prototype of an array of seven wind turbines, depicted in Fig. 14, was designed, built, and tested to compare the wind turbine array model's real performance with that of a single turbine. Different tests were conducted for varying amounts of space between the wind turbines. The results indicate that the performance of the wind turbine array is 4% less than that of a single turbine.

In the land-based wind turbine technology, the Strata Building also known as "The Razor," in London, England, is the first building in the world to incorporate wind

Fig. 12. A Concept of Wind-Powered Highway Light (inhabitat.com)

Fig. 13. Prototype Wind Turbine Model From FloDesign (businessweek.com)

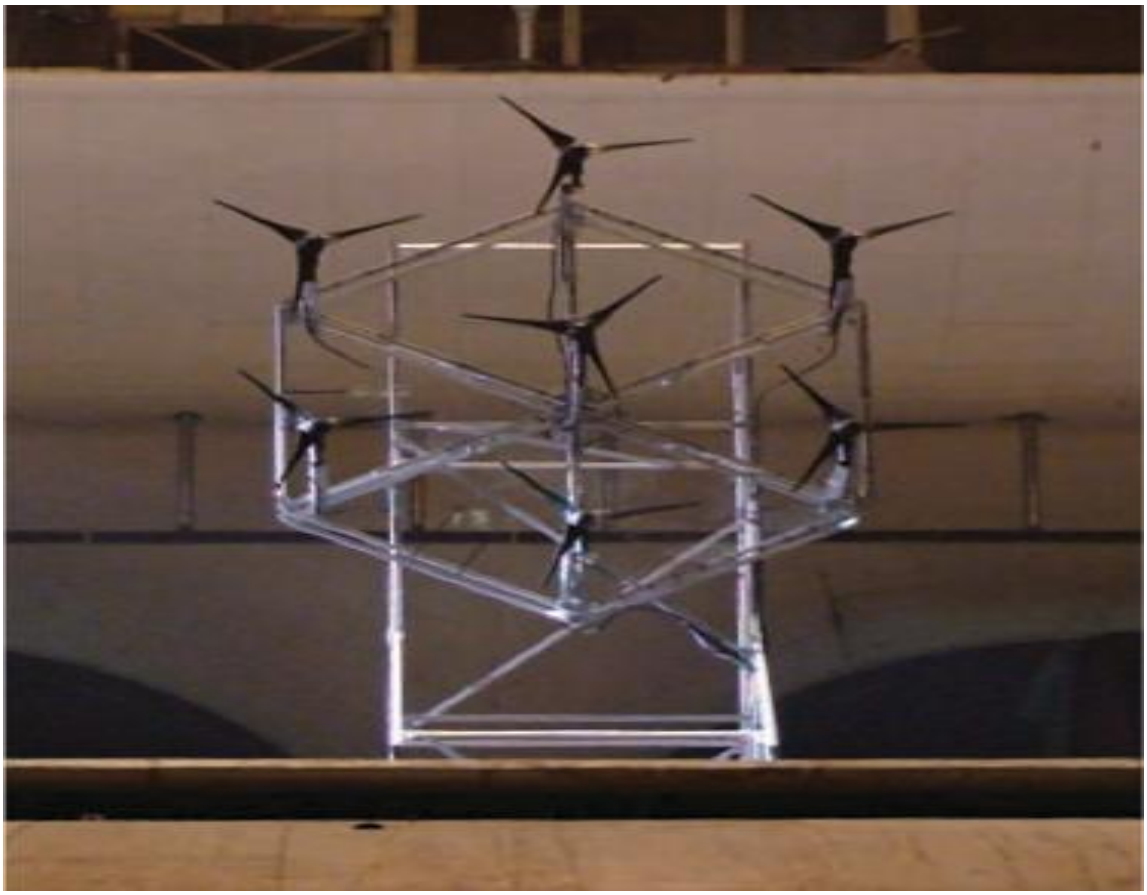

Fig. 14. A Prototype of Seven-Wind Turbines Array (Ransom and Moore 2006)

turbines into its design, as reported in Wikipedia. The building will obtain 8% of its power from three nine-meter wind turbines built into the top section of the building, as depicted in Fig. 15. Each turbine includes five blades, rather than the standard three, to reduce the noise emitted from these blades. The wind turbines are rated at 19 kW each and are expected to produce 50MW of electricity per year, an amount that will generate significant savings in the long run. The Bahrain World Trade Center is another building that incorporates wind turbines into its design structure, which includes twin towers. Each tower is 240 meters high and is linked to the other via three bridges, each of which carries a 225KW wind turbine (see Fig. 16). Wikipedia reports that these wind turbines are expected to generate 11% to 15% of the total power consumption of the twin towers. The shape of the two towers is an interesting design feature; they were designed in such a way as to provide the three wind turbines with greater wind stream. An example from dynamic architecture is David Fisher's rather unique design of a wind-powered, rotating skyscraper, which features 80 independently-rotating floors and is expected to be the world's first swirling skyscrapers (see Fig. 17). Wind turbine technology is incorporated into his design in such a way that it is hardly visible from outside and takes full advantage of the available wind around the building. A wind turbine is installed between each level for a total of 48 turbines, which together generate approximately 12 times the amount of energy needed to power the entire building. This energy can be used to power the entire area surrounding the building or can provide the power network with surplus energy. According to *The Times*, the first two such swirling skyscrapers are to be constructed in Dubai and Moscow.

One of the interesting fixed offshore wind turbine design systems is the

Fig. 15. The Strata Building in London, England (e-architech.co.uk)

Fig. 16. The Bahrain World Trade Center (wikipedia.com)

Fig. 17. David Fisher's Swirling Skyscraper (gizmag.com)

Aerogenerator X (see Fig. 18). The British company Wind Power Limited recently unveiled an innovative design of a new 10MW offshore wind turbine. The 270 m (885 ft) wide offshore wind turbine structure spins at 20 revolutions per minute and is designed as a vertical axis wind turbine. It is expected to be completed by 2014. According to the manufacturer, the Aerogenerator X will generate twice the power with only half the weight of previous designs. Another attractive floating offshore design system is the Hywind 2.3 MW Siemens wind turbine, see (Fig. 19). The Norwegian oil and gas company, Statoil, has developed and installed Hywind in the North Sea of Norway; according to the Statoil Web site, it became the world's first operational, full-scale, floating wind turbine system in the summer of 2009. Hywind is a single, floating, cylindrical spar buoy moored with three lines of catenary cables. It weighs 138 tons and has a hub height of 65 m above the sea level. Moreover, Sweden's Hexicon has developed a new futuristic design solution for offshore wind farm systems that is based on the floating platform (see Fig. 20). The conceptual design has seven large turbines and can generate up to 40 MW of renewable power, as explained on the Hexicon Web site.

1.4 Estimating Annual Energy Output

For offshore-based wind turbines, rotor diameter typically increases in proportion to hub height, as can be observed in Fig. 21. With this information, the annual energy output with respect to the Betz limit for a single offshore-based wind turbine structure can be calculated given mean wind velocity and either hub elevation or rotor diameter (see Fig. 22).

1.5 Research Objectives

The main objective of this research study is to develop basic dynamic models that can

Fig. 18. Offshore Wind Turbine, the Aerogenerator X (gizmodo.com)

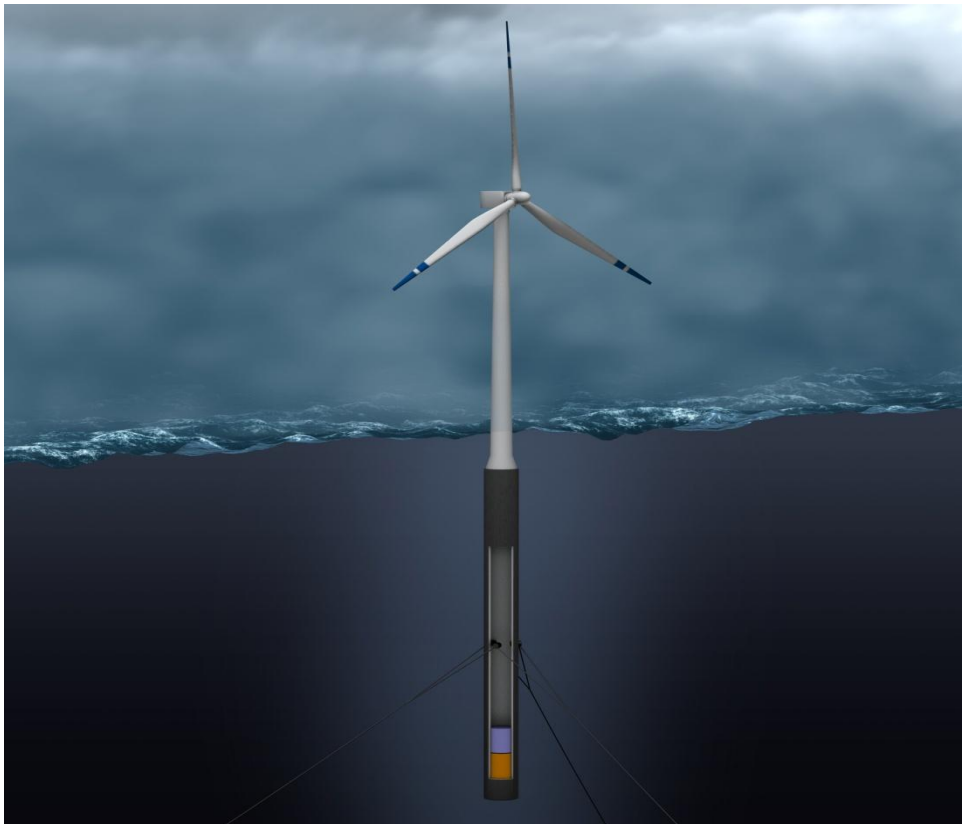

Fig. 19. Siemens Hywind Floating Wind Turbine (statoil.com)

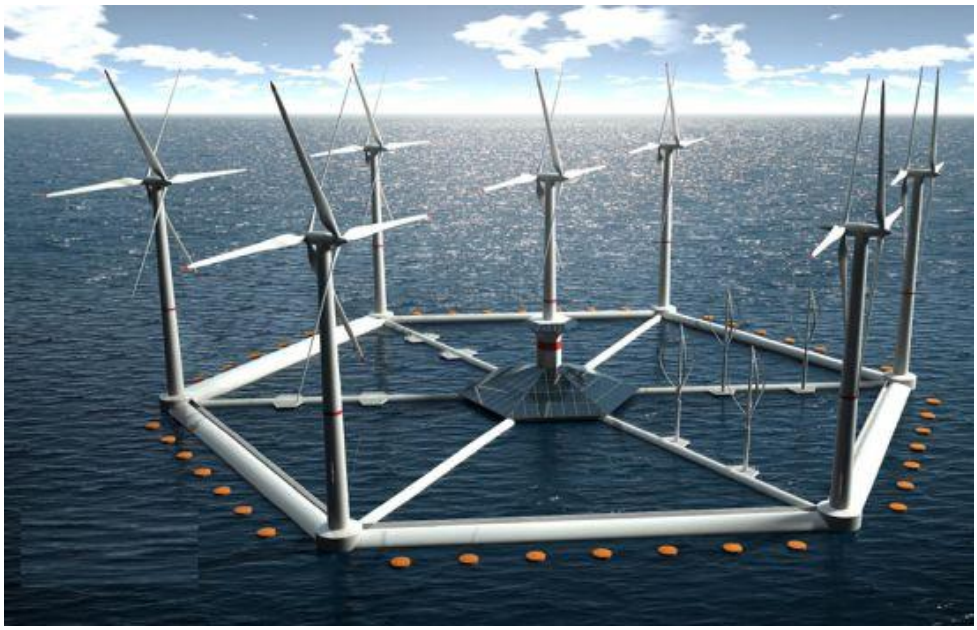

Fig. 20. A Conceptual Floating Offshore Wind Farm Design (hexicon.eu)

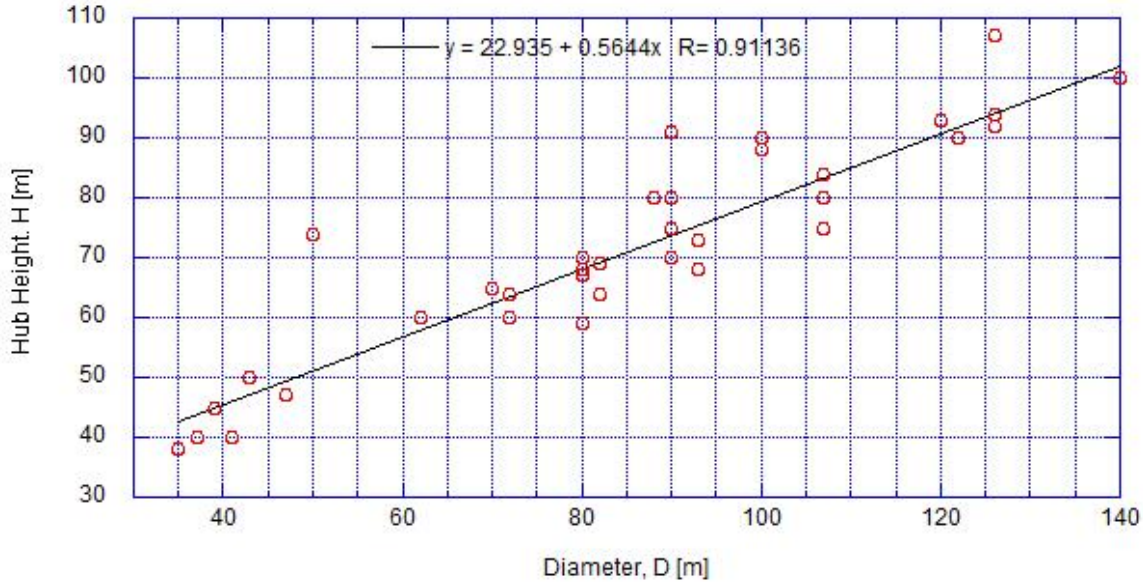

Fig. 21. The Relation Between Rotor Diameter and Hub Height for an Offshore-Based Wind Turbine Structure (Appendix-A)

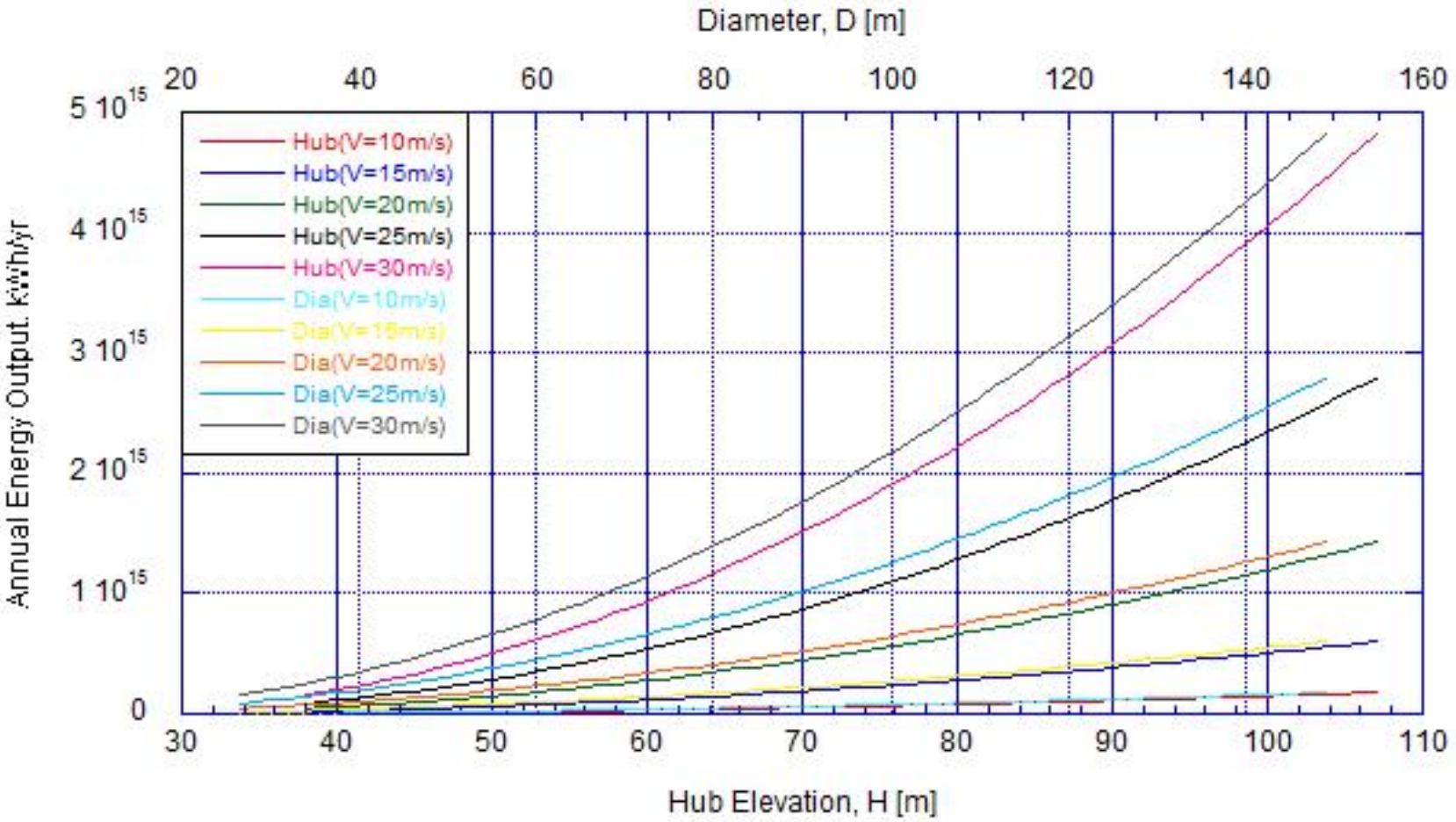

Fig. 22. The Annual Energy Output of a Single Offshore-Based Wind Turbine Structure with Respect to the Betz Limit

be used to accurately predict the response behavior of near-shore wind towers with either monopile, suction caisson, or gravity-based foundation systems. Initially two wind tower models will be investigated. The first dynamic response model to be presented addresses wind turbine with gravity based foundations and allows for sliding and rocking of the wind tower. It is based upon the earlier offshore platform model of Wilson (1984). The second dynamic response model to be presented addresses the modeling of layered soils for suction caisson foundations (Wolf and Deeks 2004). The marine hydrodynamic force model based upon the generalized Morison Equation modified to address wave and current loadings on a flexible cylindrical bottom fixed wind turbine was discussed by Merz, Moe and Gudmestad (2009). They focused on inline and transverse flow induced forces were addressed but did not include much on foundation design. In this study the environmental loads produced from the waves and currents incorporating their finding will be incorporated into the dynamic model. A refinement of the non-linear wave force model based upon the analysis for a slender cylinder by Faltinsen, Newman and Vinje (1995) will be examined. The wind loading on the slender towers will follow the usual drag force modeling techniques.

Finally, along with the development of these dynamic models, parametric studies will be performed. Simulations using these dynamic models will help us address the two and three blade offshore wind turbine systems. The applied thrust force will be developed using the NREL computer program FAST (Jonkman and Buhl Jr. 2005); or alternatively using the data from the offshore wind turbine tower with a suction caisson foundation example in (Wolf and Deeks 2004).

2. ENGINEERING APPROXIMATIONS AND BASIC MODELS

In this section, we will describe certain specific approximation techniques that can be used to estimate the natural vibration frequency of the offshore wind turbine structure (OWTS), the wake and turbulence effects, and the wave and wind forces on the structure.

2.1 Natural Vibration Frequencies

The fundamental natural frequency is one of the important dynamic criteria of the OWTS and can be estimated as (Tempel 2006):

$$f_{natural} = \sqrt{\frac{3.04}{4\pi^2}\frac{EI}{\left(m_{top} + 0.227\mu L\right)L^3}} \tag{3}$$

where, $f_{natural}, m_{top}, \mu, L, EI$ are the first natural frequency, the top mass, the tower mass per length, the tower height, and the tower bending stiffness, respectively. The formula assumes that the OWTS is a uniform beam with a top mass and a fixed based.

Vugts (1996) developed a formula for the fundamental natural frequency of a stepped shell mono-tower that can also be used for the OWTS. The formula is determined by two motions (sliding motion and rotation motion) which are assumed to be uncorrelated. By neglecting the shear effect, the fundamental natural frequency of a stepped shell mono-tower can be estimated with the following equation:

$$f_{natural} = \sqrt{\frac{3}{4\pi^2}\frac{EI_{eq}}{\left(m_{top} + m_{eq}L\right)L^3}\left[\frac{\pi^4}{48} + \frac{1}{C_{found}}\right]} \tag{4}$$

with:

$$C_{found} = \frac{3EI_{eq}}{K_{eq}L} \quad ; \quad K_{eq} = \frac{K_{rot}K_{sli}L^2}{K_{rot} + K_{sli}L^2}$$

where K_{eq} is the equivalent value of two soil stiffnesses (rotation soil stiffness = K_{rot} and

sliding soil stiffness = K_{sli}) and C_{found} is a factor related to the motion of the flexibility of the foundation. According to Vugts (1996), the C_{found} value can range from 0, which is very stiff foundation behavior, to 0.5, a rational value for flexible foundation behavior.

A more detailed method of estimating the first and second natural frequencies of a mono-tower gravity-based model from Wilson (1984) will be discussed in depth in Section 3.1.

2.2 Wake and Turbulence Considerations

Several models have been developed in an attempt to understand the behavior of turbine wakes in offshore environments. Jensen (1983) developed a basic mathematical model to calculate the energy output from multiple turbines in a wind farm. The model is based on the conservation of momentum and the velocity deficit of the wind speed.

$$U_{Deficit} = \left(1 - \frac{U}{U_0}\right) = \frac{2b}{\left(1 + 2k\frac{x}{D}\right)^2} \tag{5}$$

where U is the downstream wind speed, U_0 is the free-stream wind speed, b is the axial induction factor, k is the wake entrainment factor, x is the distance downstream, and D is the rotor diameter. The axial induction factor, b, is a function of turbine thrust coefficient C_T and can be calculated using the following formula:

$$b = \frac{1 - \sqrt{1 - C_T}}{2} \tag{6}$$

An empirical formula was developed by Frandsen (1992) to calculate the wake entrainment factor k, assuming that the hub height (z_H) and the roughness parameter of the water surface (z_0) are known.

$$k = \frac{0.5}{\ln\left(\frac{z_H}{z_0}\right)} \tag{7}$$

Certain recommendation values of the surface roughness (z_0) for the offshore wind turbine environment exist. According to Tempel (2006), Germanischer Lloyd WindEnergie GmbH (GL) recommends using $z_0 = 0.002\,m$ in their offshore wind regulations. However, the Danish guidelines advise using $z_0 = 0.001\,m$, based on the research findings of Morris et al. (2003). Different values of surface roughness parameter for various types of terrain are presented in Table 2. The surface roughness typically varies between 0.0005 *m* for rough seas condition and 0.01 *m* in coastal areas with an onshore wind.

The total wind speed deficit of wakes from multiple turbines can be calculated as follows:

$$U_{Total\ Deficit} = \left(1 - \frac{\bar{U}}{U_0}\right) = \sqrt{\sum_{i=1}^{n}\left(1 - \frac{U_i}{U_0}\right)^2} \tag{8}$$

This equation assumes that the kinetic energy loss of multiple turbines is the sum of the individual energy deficits, as set forth by Mosetti et al. (1994).

Another way of estimating the deficit is by using the regression fit from the SODAR experiment (Barthelmie et al. 2004). A curve fit was applied from the SODAR data to provide the wind speed deficits $\Delta U/U_0$ as a function of the distance from the turbine in rotor diameters *D*.

$$\Delta U/U_0 = 1.07D^{-1.11} \tag{9}$$

Magnusson and Smedman (1996) applied a similar method to onshore wakes, and

Table 2 Surface Roughness Parameter Values for Various Types of Terrain (DNV 2007)

Terrain type	Roughness parameter (m)
Plane ice	0.00001-0.0001
Open sea without waves	0.0001
Open sea with waves	0.0001-0.01
Coastal areas with onshore wind	0.001-0.01
Snow surface	0.001-0.006
Open country without significant buildings and vegetation	0.01
Mown grass	0.01
Fallow field	0.02-0.03
Long grass, rocky ground	0.05
Cultivated land with scattered buildings	0.05
Pasture land	0.2
Forests and suburbs	0.3
City centres	1-10

obtained the following relationship

$$\Delta U/U_0 = 1.03D^{-0.97} \tag{10}$$

A comparison of SODAR measurements with Magnusson and Smedman data as well as the Jensen Model, utilizing two different values of thrust coefficients C_T is presented in Fig. 23. Figs 24 (a) and 24 (b) reveal differences within the wind speed deficits among the recommended surface roughness values ($z_0 = 0.005\,m$, $z_0 = 0.001\,m$, and $z_0 = 0.002\,m$) in the Jensen model for two different thrust coefficient values. As these figures demonstrate, the critical value in estimating wind speed deficits is the thrust coefficient because it varies significantly when compared with the surface roughness value.

The distance between turbines plays a crucial role in calculating the loss in wind speed and determining the efficiency of the entire offshore wind farm. The equation for the total wind speed deficit of wakes from multiple turbines was used in Fig. 25 to demonstrate the difference in wind speed for different spacings (4D, 7D, and 10D). As indicated in the figure, the loss in wind speed is significantly less at a spacing of 10D as opposed to 4D, implying greater wind farm efficiency with 10D spacing.

Stability is one of the most important factors in wind farms. One way to describe the stability requires knowledge of the turbulence intensity at the wind turbines. Turbulence intensity is defined by

$$I = \frac{\sigma}{\bar{U}} \tag{11}$$

where σ is the standard deviation of the wind speed in the average wind direction, and $\bar{U}$ is the magnitude of the average wind speed. In order to describe the combined effect

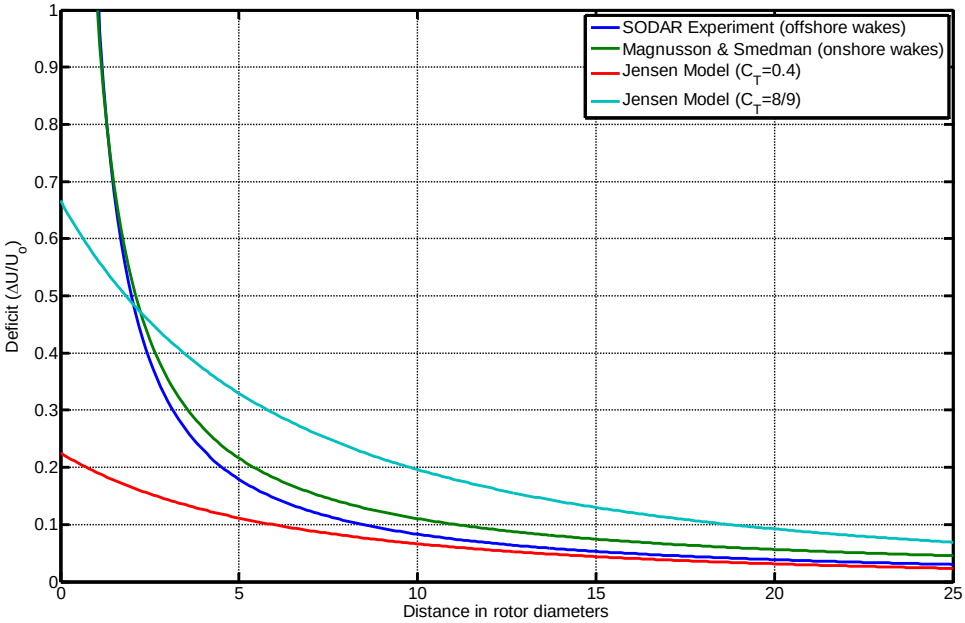

Fig. 23. Wind Speed Deficit as a Function of the Distance from the Turbine in Rotor Diameters

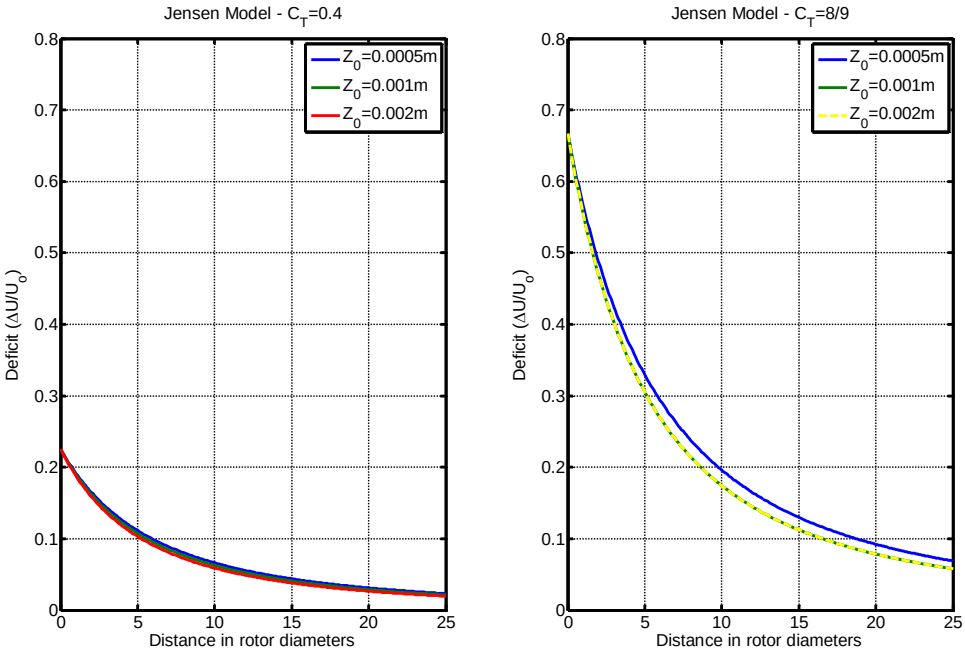

(a) (b)

Fig. 24. Wind Speed Deficits Vary with Surface Roughness Values

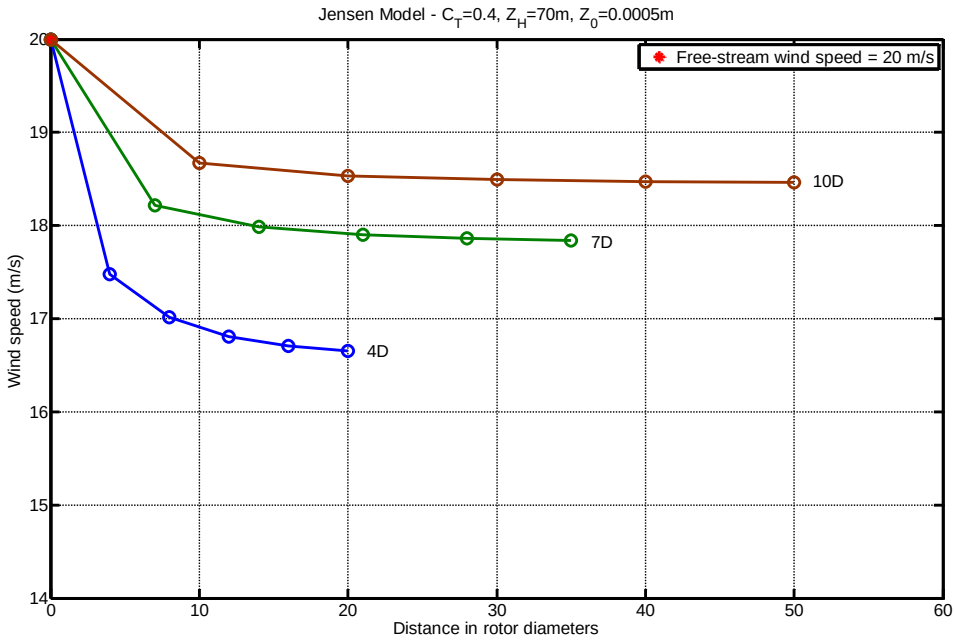

Fig. 25. The Difference in Wind Speed Loss for Different Spacing (4D, 7D, and 10D)

of the actual turbulence and wake effects, Frandsen and Thogersen (1999) developed a model for design turbulence, which allows one to estimate the equivalent turbulence (effective turbulence $= I_{eff} = \sigma_{eff} / U_{hub}$) based on the characteristics of the wind turbine material. The third edition of the international wind turbine design standard – IEC61400-1 (2005) – allow one to estimate the standard deviation of the effective turbulence (σ_{eff}), specifically

$$\sigma_{eff} = \left[\left(1 - N\ p_w\right) \sigma_a^m + p_w \sum_{i=1}^{N} \sigma_{aw}^m \right]^{1/m} \tag{12}$$

where

$$\sigma_{aw}^m = \sqrt{\frac{0.9U^2}{\left(1.5 + 0.3 s_i \sqrt{U}\right)^2} + \sigma_a^2} \quad ; \quad p_w = 0.06$$

A brief description and the units of each parameter in the above formula is presented in Table 3. This formula is only valid when the spacing between turbines is greater than or equal to 3 rotor diameters and less than 10 rotor diameters. Figs 26 (a) and 26 (b) illustrate that the turbulence intensity decreases when the wind speed or the spacing in rotor diameters between wind turbines increases.

2.3 Wave Force Models

The design of offshore structures to date has been driven by the need to recover oil and gas from offshore resources located in progressively deeper water depths. The structural excitation of these platforms is generally dominated by wave loading which can be modeled using viscous slender body or inviscid large body hydrodynamic models. Due to the complex nature of wave behavior and the variation of different shapes and sizes of offshore structures comparative experimental and numerical studies remain a

Table 3 A Brief Description of each Parameter in the Effective Turbulence Standard Deviation Formula (IEC61400-1 2005)

Parameter	Description	Units
m	Slope of S-N curve: - For blades (composites, m = 9-12) - For nacelle (cast iron, m = 6-8) - For tower (welded steel m = 3-4)	
N	Number of neighboring turbines: - For two wind turbines (N = 1) - For one row (N = 2) - For two rows (N = 5) - For inside a wind farm with more than two rows (N = 8)	
P_w	Fixed probability ($P_w = 0.06$)	
U	Wind speed at hub height	[m/s]
s_i	Distance to neighboring turbine i normalized by rotor diameter	
σ_a	Ambient turbulence	[m/s]
σ_{aw}	Combines ambient and wake tubulence	[m/s]
σ_{eff}	Effective turbulence intensity	[m/s]

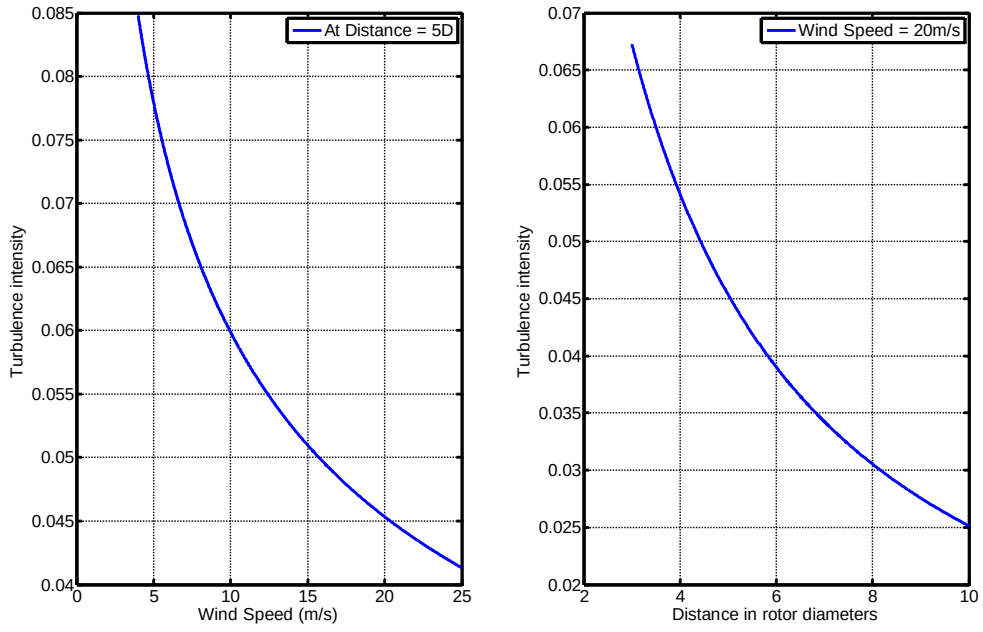

(a) (b)

Fig. 26. Turbulence Intensity Behavior

cornerstone in the design process.

2.3.1 Morison Equation

Morison et al. (1950) presented a method of estimating the wave force on piles, and this equation, which came to be referred to as the Morison equation. The hydrodynamic force on a slender structure, such as a mono-tower wind turbine structure, can be estimated using the basic Morison equation:

$$dF = dF_M + dF_D = C_M \rho \frac{\pi D^2}{4} \dot{u}\, dz + C_D \rho \frac{D}{2} |u| u dz \tag{13}$$

where the first term is related to the inertia force and the second term is related to the drag force. ρ is the water density, D is the cylinder diameter of the wind turbine tower, u is the horizontal velocity of the fluid, $\dot{u}$ is the horizontal acceleration of the fluid, and C_M and C_D are the inertia and drag coefficients, respectively. Equation (13) was developed for a fixed, or stationary, structure. However, in real life, the structure moves with respect to the velocity and acceleration of the fluid. A modified form of Morison's equation that takes relative motion with a constant current velocity into account can be expressed as

$$dF = C_M \rho \frac{\pi D^2}{4} \ddot{x}\, dz + (C_M - 1) \rho \frac{\pi D^2}{4} (\dot{u} - \ddot{x})\, dz + C_D \rho \frac{D}{2} |u + U_c - \dot{x}| (u + U_c - \dot{x})\, dz \tag{14}$$

where $\dot{x}$ is the velocity of the structure, $\ddot{x}$ is the structural acceleration, and U_c is the velocity of the current.

The key to obtaining an accurate result from Morison's equation lies in the selection of values of the inertia and drag coefficients. A detailed description of how these coefficients can be obtained from laboratory experiments is presented by Chakrabarti (1987). Merz, Moe and Gudmestad (2009) discussed the selection of coefficients for

offshore wind turbine structures, as listed in Table 4. Morison's equation, strictly speaking, is only valid when the ratio of tower diameter to wavelength is less than 0.2, that is, when the characteristic offshore structure diameter is relatively small compared to the wavelength. On the other hand, if the ratio is greater than 0.2, then the inertia force is dominant, (see Fig. 27). In this case, it is recommended that the diffraction effects become important and must be considered.

2.3.2 FNV-Theory

A more recent wave force formulation for estimating the hydrodynamic force accounting for scattering and diffraction effects was developed by Faltinsen, Newman, and Vinje. Faltinsen et al. (1995). They developed this theory in order to improve the estimation of non-linear wave forces on a fixed slender cylinder. This non-linear wave force model assumes that the wavelength is much greater than the characteristic diameter of the offshore structure. More precisely this theory assumes that the wave amplitude, A, and the cylinder radius, R, are small values compared to the wavelength L, and that both values A and R are of the same order. The diffraction regime is divided into two domains, the inner domain and the outer domain. The outer domain, which is the domain farther from the cylinder, is treated with conventional linear analysis. The inner domain which is closest to the cylinder surface, is affected by nonlinearities, results from the diffraction and scattering of the incident waves.

The general expression for the total integrated pressure force acting on the cylindrical body in the x-direction is:

$$F_x = \rho R \int_0^{2\pi} \cos\theta d\theta \int_{-h}^{0} \left(\Phi_t + \frac{1}{2} V^2 \right) dz + \rho R \int_0^{2\pi} \cos\theta d\theta \int_0^{\eta} \left(\Phi_t + \frac{1}{2} V^2 + gz \right) dz \qquad (15)$$

Based on Equation (15), the total force acting on the cylindrical body is the sum of the

Table 4 Recommended Values of C_M and C_D for Offshore Wind Turbine Structures (Morris et al. 2003)

Source	Details	Wave Only		Wave Plus Current	
		C_M	C_D	C_M	C_D
API	Recommendations for Design			1.7	1.05
Chakrabarti	Wave-tank test; 46/53 *mm* diameter		1.4	Drag dominated	1
Christchurch Bay	Offshore test; 480 *mm* diameter	1.65-1.9	0.75-0.95		
City University	Horizontal cylinder; wave tank; 210 *mm* & 500 *mm* diameter	1.2	0.6-1.2	1.2	0.6-1.2
Delta wave flume	Roughened cylinders; 216 *mm* & 513 *mm* diameter	2	1.7	1.8	1.5
DNV	Recommendations for Design	1.8	1.2		

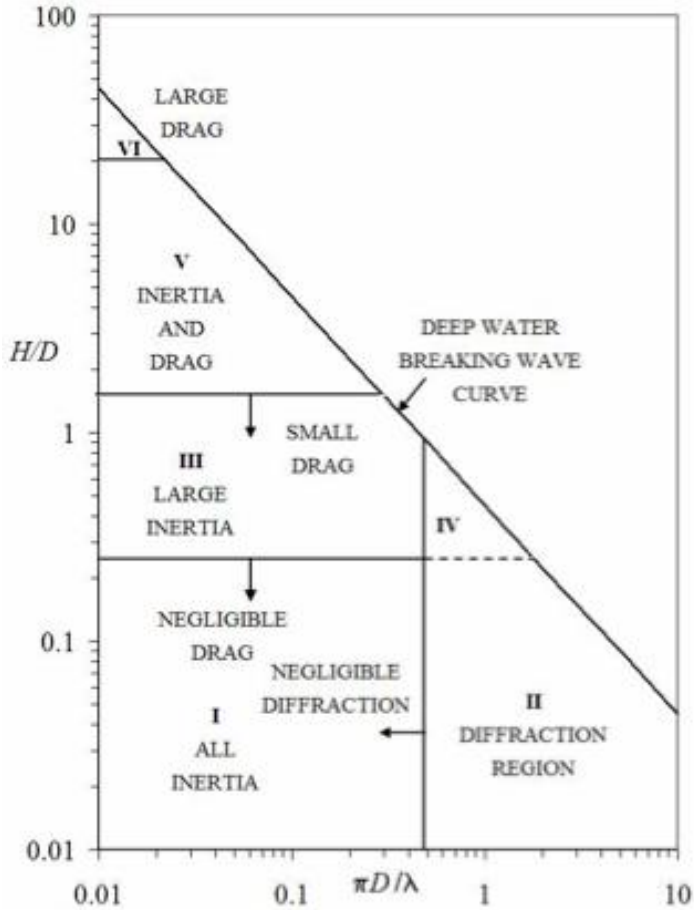

Fig. 27. Drag, Inertia, and Diffraction Wave Force Regimes (DNV 2007)

integrated forces:

$$F_x = F_{H1} + F_{H2} + F_{H3} \tag{16}$$

where

$$F_{H1} = \left[2\pi\rho g A a^2 \left(1 - e^{-Kh}\right) + \pi\rho g K^2 a^2 A^3 \right] \cos\omega t$$

$$F_{H2} = \left[\frac{1}{4} \pi\rho g K a^2 A^2 \left(1 - e^{Kh}\right) + \pi\rho g K a^2 A^2 \right] \sin 2\omega t$$

$$F_{H3} = -2\pi\rho g K^2 a^2 A^3 \cos 3\omega t$$

For more additional information regarding the forces of the FNV-theory see Faltinsen et al. (1995).

2.4 Wind Force

Aerodynamic loading on an OWTS can be viewed as being applied in two parts. The first part occurs when the wind is passing through the blades $\left(F_{blades}\right)$ and the second, when the wind is passing by the supporting tower $\left(F_{tower}\right)$ which for discussion purposes will be assumed to be of cylindrical shape.

The aerodynamic loads on the blade of the turbine can be calculated based upon blade element momentum theory, which assumes that wind flow is incompressible, homogeneous, and acts directly on the wind turbine rotor blades. According to Tempel (2006), the axial thrust force on a parked, i.e. stationary, rotor can be estimated using the following formula:

$$F_{blades} = \frac{1}{2} \rho_{air} A V^2 C_T \tag{17}$$

where ρ_{air} is the air density, A is the swept area of the rotor blades ($A = \pi D^2/4$), V is the undisturbed wind velocity, and C_T is the thrust coefficient, also referred to as the drag

coefficient by some books. The thrust coefficient (drag coefficient) can be expressed as

$$C_T = 4a(1-a) \tag{18}$$

where, a is referred to as the induction factor which is expressed as a function of two wind velocities:

$$a = \frac{V_0 - V_{disk}}{V_0} \tag{19}$$

These wind velocities are V_0 the undisturbed free stream velocity and V_{disk} the wind velocity at the actuator disk (turbine rotor). The maximum value that the induction factor can reach is 1/3, which, according to Twidell and Gaudiosi (2009), makes the maximum value of the thrust coefficient 8/9. The blades bend to deflect out of the rotor plane (flapwise bending moment) and is related to the axial thrust force can be calculated by means of the following formula:

$$M_T = \frac{F_{blades}}{B}\frac{5}{8}R \tag{20}$$

where *B* is the number of blades (usually 2-3 blades), *R* is the radius of the turbine rotor, and 5*R*/8 is the center of aerodynamic pressure for the whole blade, according to Twidell and Gaudiosi (2009).

The aerodynamic loading on the slender towers can be estimated by means of the usual drag force modeling equation:

$$F_{tower} = \frac{1}{2}\rho_{air} A V^2 C_D \tag{21}$$

where, C_D is the drag coefficient. The drag coefficient is a function of the Reynolds number (Re) and the surface roughness. For values of $\mathrm{Re} > 10^6$ the American Petroleum Institute (API) recommends a value of $C_D = 0.5$ for a cylindrical tower. Kühn et al.

(1998) illustrated a more detailed method of calculating the drag coefficient, if the slenderness ratio (λ), the Reynolds number (Re_D), the structure surface roughness (k_T), and tower diameter (D_T) are known:

$$C_D = \frac{\psi_r + 1}{2} C_{D0} \tag{22}$$

where:

$$C_{D0} = 1.2 + \frac{0.8 \log\left(10 k_T / D_T\right)}{1 + 0.4 \log\left(\mathrm{Re}_D / 10^6\right)}$$

and

$$\psi_r = \frac{1}{90}\left(\lambda + 53\right) \quad \text{for} \quad \lambda \le 10$$

$$\psi_r = \frac{1}{360}\left(\lambda + 242\right) \quad \text{for} \quad \lambda \le 10$$

The slenderness ratio is the ratio of the height of the support structure, from mean seawater level to the base of the nacelle, divided by the tower diameter.

3. MORE DETAILED MATHEMATICAL MODELS

3.1 Gravity Based Foundation Model (Frequency Domain)

A gravity foundation is designed to resist rotation and sliding induced by ocean waves, subsea ocean currents, and wind loads. A schematic of an idealized gravity structure is shown in Fig. 28, and the corresponding soil-disk model is shown in Fig. 29. By applying Newton's second law, $\overset{+}{\rightarrow}\sum F = ma$ and moment equation $\overset{+}{\curvearrowleft}\sum M_{about-G} = J_G\ddot{\theta}$, about the center of mass center of the gravity based structure, G, to formulate the equations of motion, one obtains the following coupled equations of motion (Wilson 1984):

$$\overbrace{\begin{bmatrix} m & 0 \\ 0 & J_G \end{bmatrix}}^{M}\overbrace{\begin{bmatrix} \ddot{\upsilon} \\ \ddot{\theta} \end{bmatrix}}^{\ddot{\xi}} + \overbrace{\begin{bmatrix} \frac{J_o}{J_G}c_1 & -\frac{mh_G}{J_G}c_0 \\ -h_G c_1 & c_0 \end{bmatrix}}^{C}\overbrace{\begin{bmatrix} \dot{\upsilon} \\ \dot{\theta} \end{bmatrix}}^{\dot{\zeta}} + \overbrace{\begin{bmatrix} \frac{J_o}{J_G}k_1 & -\frac{mh_G}{J_G}\left(k_0 - m_o g h_G + m_b g h_b\right) \\ -h_G k_1 & \left(k_0 - m_o g h_G + m_b g h_b\right) \end{bmatrix}}^{K}\overbrace{\begin{bmatrix} \upsilon \\ \theta \end{bmatrix}}^{\zeta}$$

$$= \overbrace{\begin{bmatrix} \left[1 - \frac{mh_G}{J_G}\left(h_o - h_G\right)\right]F(t) - \frac{mh_G}{J_G}M_G(t) \\ M_G(t) + \left(h_o - h_G\right)F(t) \end{bmatrix}}^{F} \tag{23}$$

In general modeling the soil resistance is quite complicated and here the soil is assumed to be a homogeneous, uniform, that can be modeled as elastic half-space. (Nataraja and Kirk 1977). They developed the following model from which the soil stiffness of sliding (k_1) and rotation (k_0) and the soil radiation damping of sliding (c_1) and rotation (c_0) can be calculated:

$$k_1 = \frac{8G_S}{2-\nu}\left(1 - 0.05\omega r_0\sqrt{\frac{\rho_S}{G_S}}\right)r_0 \tag{24}$$

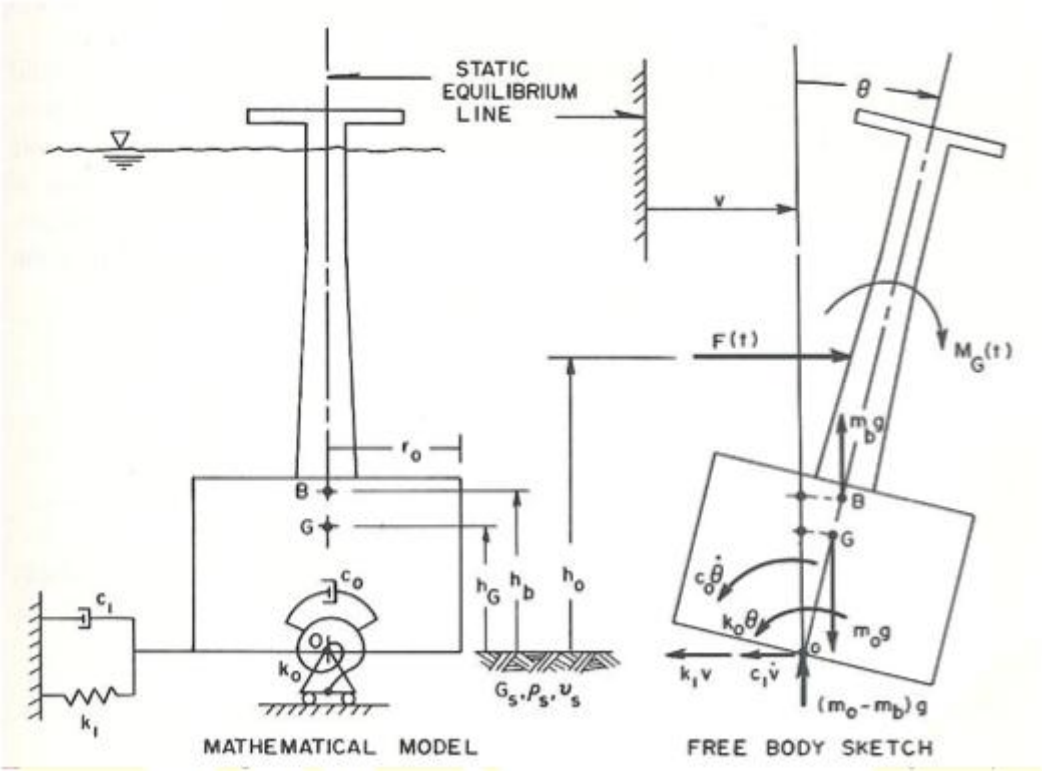

Fig. 28. Idealizations Used to Model an Offshore Gravity-Based Platform (Wilson 1984)

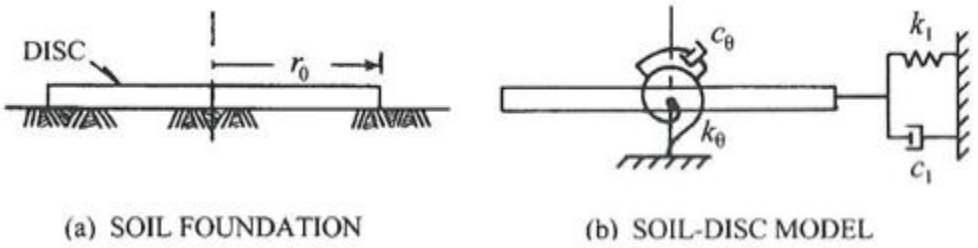

Fig. 29. Soil Foundation Models for Gravity-Based Offshore Platform (Wilson 1984)

$$k_0 = \frac{8G_S}{3(1-\nu)}\left(1-0.215\,\omega r_0\sqrt{\frac{\rho_S}{G_S}}\right)r_0^3 \tag{25}$$

$$c_1 = \frac{8}{2-\nu}\sqrt{\rho_S G_S}\left(0.67-0.02\,\omega r_0\sqrt{\frac{\rho_S}{G_S}}\right)r^2 \tag{26}$$

$$c_0 = \frac{0.375}{1-\nu}\omega\rho_S r_0^5 \tag{27}$$

where ω is the fundamental disk frequency, G_S is the soil shear modulus, ν is Poisson's ratio, and ρ_S is the soil mass density. As each of these coefficients is a function of frequency, an iterative solution is required. Wilson (1984) obtained an initial trial frequency by estimating the free undamped rocking frequency for the gravity platform to obtain the initial eigen solution, i.e. the frequencies, mode shapes. Then it is simply a matter of iterating until the eigenvalues converge. If desired the environmental forces (waves, current and wind forces) can be applied to the structure, damping can be applied to the system, and the response behavior can be evaluated using for example mixed time-frequency domain methods.

3.2 Suction Caisson Foundation Model (Frequency Domain)

The suction caisson model is based on a theory for conical bars and beams that was developed to solve foundation vibration problems, specifically the dynamic analysis of surface foundations. Wolf and Meek (1994) extended the cone models to represent embedded foundations, which can be used to analyze both monopile and suction caisson foundations in multiple-layered half-space. In this foundation model, the horizontal, vertical, rocking, torsional, and coupling dynamic-stiffness coefficients $S(a_0) = K\left(k(a_0) + i\,a_0 c(a_0)\right)$ of the particular offshore site are estimated. The variables

$K, k(a_0), a_0,$ and $c(a_0)$ are the static-stiffness coefficient, the dimensionless spring coefficient, the dimensionless frequency, and the dimensionless damping coefficient, respectively. Wolf and Deeks (2004) used this methodology to analyze the dynamic response of an offshore wind turbine tower with a suction caisson foundation (see Fig. 30). This particular model was based on a design from the Swedish Opti-OWECS project that utilized a two-blade wind turbine (Kühn et al. 1998). First, the net horizontal wind force acting on the structure and the horizontal, rocking, and coupling dynamic-stiffness coefficients for the site ($S_h(\omega), S_r(\omega),$ and $S_{hr}(\omega)$) were calculated based on wave propagation in cones. This was incorporated into the equations of motion:

$$\begin{aligned}
&\sum F_{Z=h} = V(\omega_j) \Rightarrow -\omega_j^2 m_1 \left[u_0(\omega_j) + h\vartheta_0(\omega) + u(\omega_j) \right] + k(1+2\zeta i) u(\omega_j) = V(\omega_j) \\
&\sum F_{Z=0} = V(\omega_j) \Rightarrow -\omega_j^2 m_2 u_0(\omega_j) - \omega_j^2 m_1 \left[u_0(\omega_j) + h\vartheta_0(\omega) + u(\omega_j) \right] \\
&+ S_h(\omega_j) u_0(\omega_j) + S_{hr}(\omega_j) \vartheta_0(\omega_j) = V(\omega_j) \\
&\sum M_{Z=0} = hV(\omega_j) \Rightarrow -\omega_j^2 I \vartheta(\omega_j) - \omega_j^2 m_1 h \left[u_0(\omega_j) + h\vartheta_0(\omega) + u(\omega_j) \right] \\
&+ S_{rh}(\omega_j) u_0(\omega_j) + S_r(\omega_j) \vartheta_0(\omega_j) = hV(\omega_j)
\end{aligned} \tag{28}$$

The suction caisson foundation model indicated in Fig. 31 has a three-degrees-of – freedom (3-DOF) system. The formulation and solution were carried out in the frequency domain. and the displacement and rotation amplitudes at different frequencies were thus obtained. For additional information regarding the suction caisson foundation model, see Wolf and Deeks (2004).

3.3 Finite Element Model (Time Domain)

Analytical methods are do not yield closed-form solutions for many complex problems and consequently discrete element methods such as the finite element method is

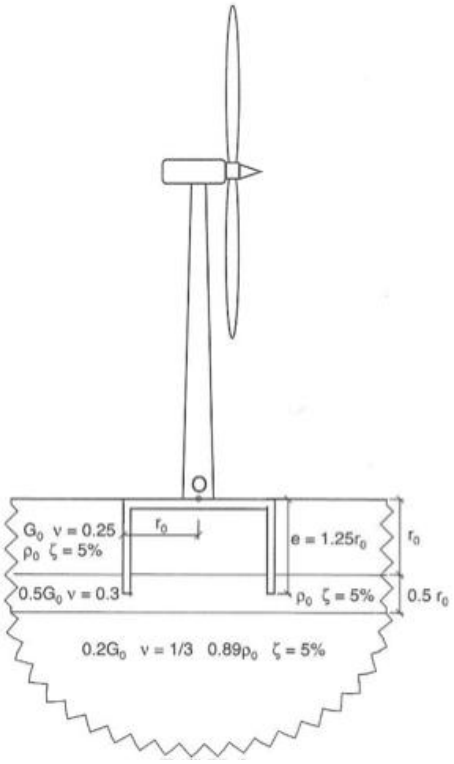

Fig. 30. Schematic of a Suction Caisson Wind Tower Model in a Layered Soil (Wolf and Deeks 2004)

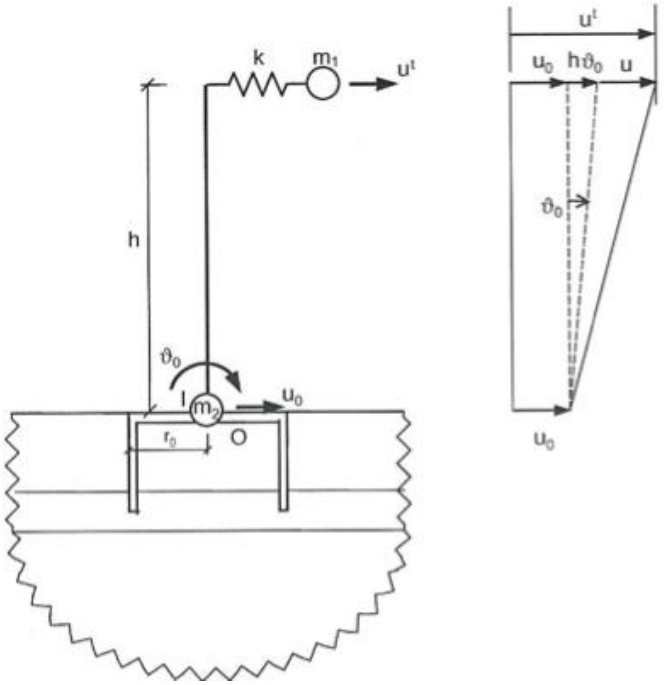

Fig. 31. Three-Degrees-Of- Freedom System (3-DOFS) of Wind Turbine Structure (Wolf and Deeks 2004)

used to obtain numerical solutions in many scientific and engineering applications.

The finite element method is quite versatile and has been applied to all kinds of structural systems, including the analysis of wind turbines (Lavassas et al. 2003). A wind turbine tower can be modeled as a series multiple beam elements connected to one another at nodal points. Consider a two-dimensional beam element and that has a uniform cross-sectional moment of inertia *I*, material modulus of elasticity *E*, and length *L*. Each beam element has two nodes, and each node has two degrees of freedom, i.e. rotation and displacement. The stiffness and consistent mass matrices of this beam element can be expressed as (see for example Kwon and Bang 2000):

$$[K]=\begin{bmatrix} k_{11} & k_{12} & k_{13} & k_{14} \\ k_{21} & k_{22} & k_{23} & k_{24} \\ k_{31} & k_{32} & k_{33} & k_{34} \\ k_{41} & k_{42} & k_{43} & k_{44} \end{bmatrix} = \frac{EI}{L^3}\begin{bmatrix} 12 & 6L & -12 & 6L \\ 6L & 4L^2 & -6L & 2L^2 \\ -12 & -6L & 12 & -6L \\ 6L & 2L^2 & -6L & 4L^2 \end{bmatrix} \tag{29}$$

where

$$k_{ij} = \int_0^L EI\psi_i''(x)\psi_j''(x)\,dx$$

and,

$$\psi_1(x) = 1-3\left(\frac{x}{L}\right)^2+2\left(\frac{x}{L}\right)^3$$

$$\psi_2(x) = x\left(1-\frac{x}{L}\right)^2$$

$$\psi_3(x) = 3\left(\frac{x}{L}\right)^2-2\left(\frac{x}{L}\right)^2$$

$$\psi_4(x) = \frac{x^2}{L}\left(\frac{x}{L}-1\right)$$

And the consistent mass matrix of the beam element can be expressed as:

$$[M]=\begin{bmatrix} m_{11} & m_{12} & m_{13} & m_{14} \\ m_{21} & m_{22} & m_{23} & m_{24} \\ m_{31} & m_{32} & m_{33} & m_{34} \\ m_{41} & m_{42} & m_{43} & m_{44} \end{bmatrix} = \frac{\rho AL}{420}\begin{bmatrix} 156 & 22L & 54 & -13L \\ 22L & 4L^2 & 13L & -3L^2 \\ 54 & 13L & 156 & -22L \\ -13L & -3L^2 & -22L & 4L^2 \end{bmatrix} \tag{30}$$

where,

$$m_{ij} = \int_0^L m(x)\psi_i(x)\psi_j(x)\,dx \quad ; \quad m(x) = \rho A$$

Note that ρ is material mass density and A is the cross-sectional area of the element. For additional information about the element stiffness coefficient and the consistent mass coefficient.

Another means of defining the mass properties of the structure is to assume that the entire mass of the element is concentrated at the nodes. Assuming that there is no rotational inertia at these nodes, the inertial effect associated with any rotational degree of freedom is zero. Otherwise, the inertial effect should be accounted for by calculating the mass moment of inertia (J) of the beam element. The final form of the matrix, referred to as the lumped mass matrix can then be expressed as:

$$[M]=\begin{bmatrix} m_1 & 0 & 0 & 0 \\ 0 & J_1 & 0 & 0 \\ 0 & 0 & m_2 & 0 \\ 0 & 0 & 0 & J_2 \end{bmatrix} \tag{31}$$

For additional information regarding the lumped mass matrix, see for example Paz (1997).

All structures in motion dissipate energy and the rate of energy dissipation causing vibrational decay over time is termed damping. The energy dissipated can be a result of hysteresis losses within the material of the structure, viscous energy losses in the

surrounding water and soil, and frictions in structural joints or some combination of each. Therefore, it is often easier to estimate the effective damping of the structure. The damping coefficients c_{ij} for the structure can be estimated using the following equation:

$$c_{ij} = \int_0^L c(x)\psi_i(x)\psi_j(x) \tag{32}$$

where, $c(x)$ is the distributed viscous damping property. The damping is usually expressed in terms of an experimentally determined or estimated critical damping ratio (ξ) rather than attempting to explicitly evaluating the damping property $c(x)$. One of the methods of evaluating the effect of viscous damping entails assuming the damping matrix to be proportional to the combination of the mass and stiffness matrices (Clough and Penzien's, 1975). This method is referred to as Rayleigh damping or proportional damping:

$$[C] = a_0[M] + a_1[K] \tag{33}$$

where a_0 and a_1 are Rayleigh damping factors and can be evaluated from the expression:

$$\begin{bmatrix} a_0 \\ a_1 \end{bmatrix} = \frac{2\omega_1\omega_2}{\omega_2^2 - \omega_1^2} \begin{bmatrix} \omega_2 & -\omega_1 \\ -\frac{1}{\omega_2} & \frac{1}{\omega_1} \end{bmatrix} \begin{bmatrix} \xi_1 \\ \xi_2 \end{bmatrix} \tag{34}$$

where ω_1 and ω_2 refer to the first and second natural frequencies. However, if the damping ratio is assured to be constant for each mode, i.e. $\xi = \xi_1 = \xi_2$, then the Rayleigh damping factors may be evaluated using the simplified form:

$$\begin{bmatrix} a_0 \\ a_1 \end{bmatrix} = \frac{2\xi}{\omega_1 + \omega_2} \begin{bmatrix} \omega_1\omega_2 \\ 1 \end{bmatrix} \tag{35}$$

For additional information on the proportional damping matrix, see for example

Paz (1997) or Yang et al. (2004).

Since the foundation represents approximately 15% to 40% of the cost of an offshore wind turbine structure installation (Byrne and Houlsby, 2000), the selection of pile, suction caisson, or gravity-type system is an important design consideration and is dependent upon such soil characteristics as strength and stability. A simplified approach to address monopile-soil interaction, is to utilize the concept of the Apparent Fixity Level (AFL). This approach assumes that the monopile is fixed at a certain distance beneath the seabed, termed "effective embedment". This model is usually used to perform a preliminary dynamic analysis of the structure and offers a good engineering approximation in the absence of detailed information on the actual soil properties. The AFL is estimated as a function of the soil type surrounding the monopile structure and is specified as a multiple of the pile diameter of the structure. Some typical values are given in Table 5. The Randolph elastic continuum model offers another method by which to describe the pile-soil interaction behavior. The model can be expressed in a stiffness matrix with the following equations:

$$[K] = \begin{bmatrix} k_{xx} & k_{x\theta} \\ k_{\theta x} & k_{\theta\theta} \end{bmatrix} \tag{36}$$

where

$$k_{xx} = 4.52 m^* r_o^2 \left[\frac{E_P}{m^* r_o} \right]^{\left(\frac{1}{3}\right)} \quad ; \quad k_{x\theta} = k_{\theta x} = -2.4 m^* r_o^3 \left[\frac{E_P}{m^* r_o} \right]^{\left(\frac{5}{9}\right)} \quad ; \quad k_{\theta\theta} = 2.16 m^* r_o^4 \left[\frac{E_P}{m^* r_o} \right]^{\left(\frac{7}{9}\right)}$$

and

$$E_p = \frac{EI}{\frac{1}{64}\pi D^4} \quad ; \quad m^* = m.\left(1 + \frac{3}{4}\nu\right)$$

where $E, I, D, m, \nu,$ and r_o refer to the modulus of elasticity of the pile material, the

Table 5 Suggestions for Apparent Fixity Level (Zaaijer 2002)

Configuration	Apparent Fixity Level (AFL)
Stiff clays	$3.5D - 4.5D$
Very soft silts	$7D - 8.5D$
In the absence of all other data	$6D$
From measurement of an offshore turbine (500 kW)	$3.3D - 3.7D$

moment of inertia of the pile cross-section, the pile diameter, the rate of change of the soil shear modulus, the Poisson's ratio of the soil layer, and the outer radius of the pile, respectively. This linear model has no damping effect and assumes the pile to be longer than a critical pile length (L_c):

$$L_c = 2r_o.\left(\frac{E_p}{m^*.r_o}\right)^{\left(\frac{2}{9}\right)} \tag{37}$$

For additional information regarding the Randolph elastic continuum model, see Randolph (1981).

The natural state of the soil is rarely linearly homogeneous and usually consists of different layers, each of possessing different soil properties and it is therefore important to consider this affect in estimating the dynamic response of a wind turbine tower. The modified cone models can be utilized to evaluate the dynamic behavior of foundations consisting of multiple layers of soil. Originally, the cone model was developed to analyze the dynamic behavior of surface foundations under translational and rotational motions. Wolf and Meek (1994) extended the cone models to represent embedded foundations, such as monopile and suction caisson foundations in multiple-layered half-space, by calculating the sliding (S_h), rotation (S_r), and coupling $(S_{hr} = S_{rh})$ dynamic-stiffness coefficients. In their analysis the foundation is represented by a series stack of disks and the dynamic-stiffness coefficients $\left(S_{00}^{g}(\omega)\right)$ can be calculated by the following formula in matrix form:

$$\left[S_{00}^{g}(\omega)\right] = \begin{bmatrix} S_h & S_{hr} \\ S_{rh} & S_r \end{bmatrix} = [AH]^T\left[S_u^f(\omega)\right][AH] + [AR]^T\left[S_g^f(\omega)\right][AR] + \omega^2[M] \tag{38}$$

where,

$$[M]=\pi r_0^2\begin{bmatrix} d_1\rho_1+(e-d_1)\rho_2 & d_1\left(e-\frac{d_1}{2}\right)\rho_1+\frac{(e-d_1)^2}{2}\rho_2 \\ d_1\left(e-\frac{d_1}{2}\right)\rho_1+\frac{(e-d_1)^2}{2}\rho_2 & d_1\rho_1\left(e^2-ed_1+\frac{d_1^2}{3}+\frac{r_0^2}{4}\right)+(e-d_1)\rho_2\left(\frac{(e-d_1)^2}{3}+\frac{r_0^2}{4}\right) \end{bmatrix}$$

In equation (38) $[AH]$ refers to the upper portion and $[AR]$ to the lower portion of the kinematic-constraint matrix $[A]$of the rigid foundation, $\left[S_u^f(\omega)\right]$ and $\left[S_\vartheta^f(\omega)\right]$represent the dynamic-stiffness matrix of the free field in the frequency domain for horizontal and rocking motions, respectively, and $[M]$ stands for the rigid-body mass matrix for horizontal and rocking motions (see Fig. 32). For additional information about dynamic-stiffness coefficient formulas, see Wolf and Deeks (2004).

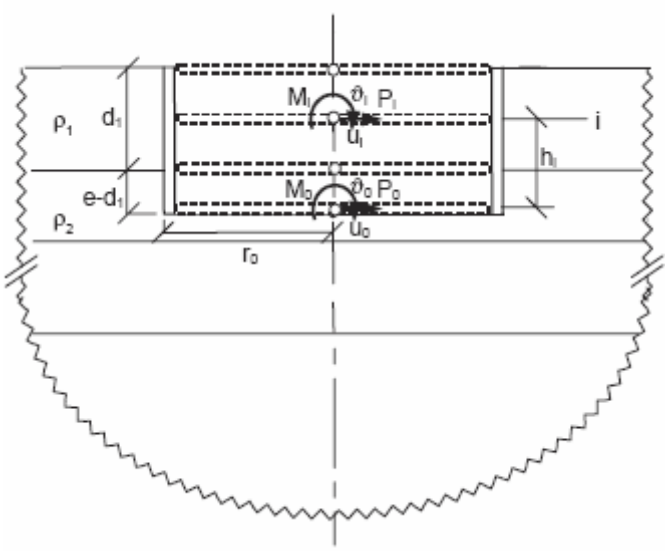

Fig. 32. Rigid-Body Mass for Horizontal and Rocking Motions (Wolf and Deeks 2004)

4. NUMERICAL SIMULATIONS

4.1 Finite Element Model (Time Domain)

A finite element model was developed that allows for the introduction of three different soil foundation models, wave force excitation and wind thrust excitation on a mono-tower. Starting first at the foundation of the structure, the apparent fixity level (AFL), Randolph elastic continuum, and modified cone models are used for evaluating the soil stiffness effects on the dynamic response of a monopile wind turbine structure. The use of these models allows for the variation of soil properties with depth below the seafloor to be more accurately addressed. In the numerical simulations the soil is initially assumed to be a stiff clay uniform over the depth of the foundation for each of the foundation models. The soil properties for the three layer model are presented in Fig. 33. The wave forces on mono-tower are estimated using the Morison's wave force equation (Morison et al. 1950) and the newer FNV method (Faltinsen et al. 1995). The wind force on the slender tower is estimated using the standard drag force equation. The thrust force developed by the three blade configurations are obtained from NREL's FAST Software. The two bladed configuration thrust force is based upon the idealized thrust signal presented by Wolf and Deeks (2004). The time domain integration of the wind turbine models was performed using Newmark-Beta Method (Newmark 1959) and was implemented in MATLAB Software.

4.2 Monopile Wind Turbine Structure (1.5 MW) Unit

The wind turbine is assumed to be cantilevered about the AFL as depicted in Fig. 34. Assuming that the soil at the site is a stiff clay, then according to Table 5, the length of the first element is estimate to be 13 m, as shown in Fig. 34. The rest of the number of beam elements and their lengths can be varied but are limited here for illustrative

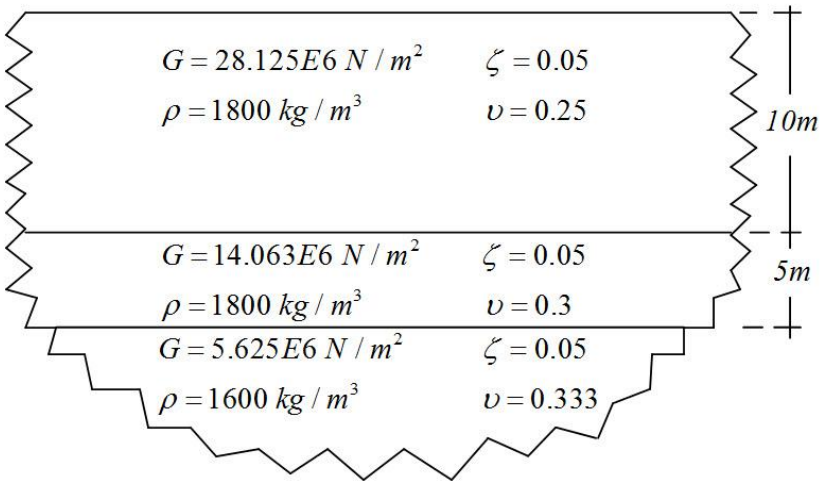

Fig. 33. Soil Properties of the Three Layers (Wolf and Deeks 2004)

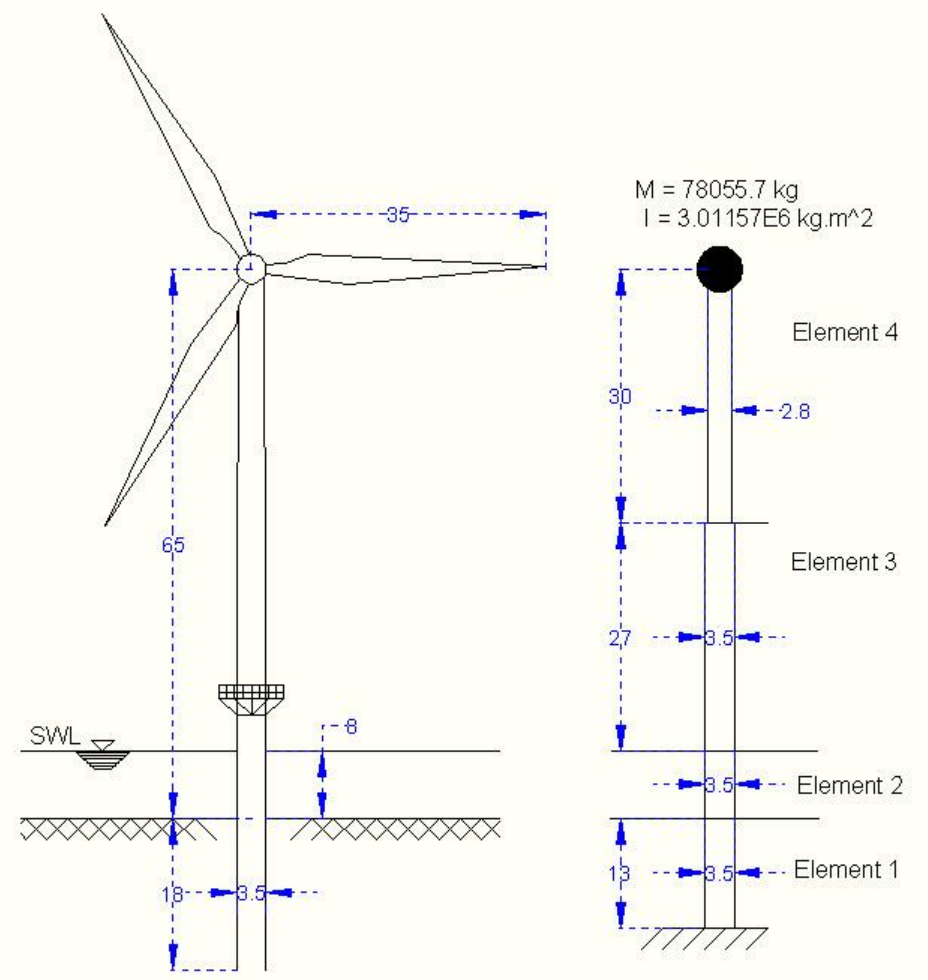

Fig. 34. Dimensions and Elements of Monopile Offshore Wind Turbine Structure (1.5 MW) Unit for the AFL Model

purposes. The lumped mass matrix is used for the upper part of the structure (rotor + nacelle), see equation (31), and added to the last element of the matrix. The general final element stiffness matrix and element mass matrix forms for the AFL model are explicitly presented in Fig. 35. Note that the first two rows and columns of the final matrix form of the AFL model will be zeros because of the fixed point at the bottom of the structure.

In the Randolph elastic continuum model, the finite element model has three elements (see Fig. 36). As Randolph's model offers another method of describing the pile-soil interaction behavior, that is, with the model's stiffness matrix, equation (36) is added to the upper part of the matrix system, as shown in Fig. 37. In addition, the lumped mass matrix is used for the lower part of the structure (monopile foundation) and added to the first element of the matrix. The rest of the elements are treated in the same way as in the AFL model. The general final matrix form of the Randolph's model is shown in Fig. 37.

The modified cone model describes the soil behavior by estimating the sliding $\left(S_h\right)$, rotation $\left(S_r\right)$, and coupling $\left(S_{hr}=S_{rh}\right)$ dynamic-stiffness coefficients. The dynamic-stiffness coefficient is given by the following:

$$S\left(a_0\right)=K\left[k\left(a_0\right)+ia_0c\left(a_0\right)\right] \tag{39}$$

where

$$a_0=\frac{\omega r_0}{c_S} \quad ; \quad c_S=\sqrt{\frac{G_S}{\rho_S}}$$

K is the static-stiffness coefficient, $k\left(a_0\right)$ is the dimensionless spring coefficient, a_0 is the dimensionless frequency, r_0 is the radius of the foundation, c_S is the shear-wave

$$[M]=\begin{bmatrix}
\frac{13\rho_1A_1L_1}{35} & \frac{11\rho_1A_1L_1^2}{210} & \frac{54\rho_1A_1L_1}{420} & \frac{-13\rho_1A_1L_1^2}{420} & 0 & 0 & 0 & 0 & 0 & 0\\
\frac{11\rho_1A_1L_1^2}{210} & \frac{\rho_1A_1L_1^3}{105} & \frac{13\rho_1A_1L_1^2}{420} & \frac{-3\rho_1A_1L_1^3}{420} & 0 & 0 & 0 & 0 & 0 & 0\\
\frac{54\rho_1A_1L_1}{420} & \frac{13\rho_1A_1L_1^2}{420} & \frac{13\left(\rho_1A_1L_1+\rho_2A_2L_2\right)}{35} & \frac{11\left(\rho_2A_2L_2^2-\rho_1A_1L_1^2\right)}{210} & \frac{54\rho_2A_2L_2}{420} & \frac{-13\rho_2A_2L_2^2}{420} & 0 & 0 & 0 & 0\\
\frac{-13\rho_1A_1L_1^2}{420} & \frac{-3\rho_1A_1L_1^3}{420} & \frac{11\left(\rho_2A_2L_2^2-\rho_1A_1L_1^2\right)}{210} & \frac{\left(\rho_1A_1L_1^3+\rho_2A_2L_2^3\right)}{105} & \frac{13\rho_2A_2L_2^2}{420} & \frac{-3\rho_2A_2L_2^3}{420} & 0 & 0 & 0 & 0\\
0 & 0 & \frac{54\rho_2A_2L_2}{420} & \frac{13\rho_2A_2L_2^2}{420} & \frac{13\left(\rho_2A_2L_2+\rho_3A_3L_3\right)}{35} & \frac{11\left(\rho_3A_3L_3^2-\rho_2A_2L_2^2\right)}{210} & \frac{54\rho_3A_3L_3}{420} & \frac{-13\rho_3A_3L_3^2}{420} & 0 & 0\\
0 & 0 & \frac{-13\rho_2A_2L_2^2}{420} & \frac{-3\rho_2A_2L_2^3}{420} & \frac{11\left(\rho_3A_3L_3^2-\rho_2A_2L_2^2\right)}{210} & \frac{\left(\rho_2A_2L_2^3+\rho_3A_3L_3^3\right)}{105} & \frac{13\rho_3A_3L_3^2}{420} & \frac{-3\rho_3A_3L_3^3}{420} & 0 & 0\\
0 & 0 & 0 & 0 & \frac{54\rho_3A_3L_3}{420} & \frac{13\rho_3A_3L_3^2}{420} & \frac{13\left(\rho_3A_3L_3+\rho_4A_4L_4\right)}{35} & \frac{11\left(\rho_4A_4L_4^2-\rho_3A_3L_3^2\right)}{210} & \frac{54\rho_4A_4L_4}{420} & \frac{-13\rho_4A_4L_4^2}{420}\\
0 & 0 & 0 & 0 & \frac{-13\rho_3A_3L_3^2}{420} & \frac{-3\rho_3A_3L_3^3}{420} & \frac{11\left(\rho_4A_4L_4^2-\rho_3A_3L_3^2\right)}{210} & \frac{\left(\rho_3A_3L_3^3+\rho_4A_4L_4^3\right)}{105} & \frac{13\rho_4A_4L_4^2}{420} & \frac{-3\rho_4A_4L_4^3}{420}\\
0 & 0 & 0 & 0 & 0 & 0 & \frac{54\rho_4A_4L_4}{420} & \frac{13\rho_4A_4L_4^2}{420} & \frac{13\rho_4A_4L_4}{35}+M & \frac{-11\rho_4A_4L_4^2}{210}\\
0 & 0 & 0 & 0 & 0 & 0 & \frac{-13\rho_4A_4L_4^2}{420} & \frac{-3\rho_4A_4L_4^3}{420} & \frac{-11\rho_4A_4L_4^2}{210} & \frac{\rho_4A_4L_4^3}{105}+I
\end{bmatrix}$$

$$[K]=\begin{bmatrix}
\frac{12EI_1}{L_1^3} & \frac{6EI_1}{L_1^2} & \frac{-12EI_1}{L_1^3} & \frac{6EI_1}{L_1^2} & 0 & 0 & 0 & 0 & 0 & 0\\
\frac{6EI_1}{L_1^2} & \frac{4EI_1}{L_1} & \frac{-6EI_1}{L_1^2} & \frac{2EI_1}{L_1} & 0 & 0 & 0 & 0 & 0 & 0\\
\frac{-12EI_1}{L_1^3} & \frac{-6EI_1}{L_1^2} & \frac{12EI_1}{L_1^3}+\frac{12EI_2}{L_2^3} & \frac{-6EI_1}{L_1^2}+\frac{6EI_2}{L_2^2} & \frac{-12EI_2}{L_2^3} & \frac{6EI_2}{L_2^2} & 0 & 0 & 0 & 0\\
\frac{6EI_1}{L_1^2} & \frac{2EI_1}{L_1} & \frac{-6EI_1}{L_1^2}+\frac{6EI_2}{L_2^2} & \frac{4EI_1}{L_1}+\frac{4EI_2}{L_2} & \frac{-6EI_2}{L_2^2} & \frac{2EI_2}{L_2} & 0 & 0 & 0 & 0\\
0 & 0 & \frac{-12EI_2}{L_2^3} & \frac{-6EI_2}{L_2^2} & \frac{12EI_2}{L_2^3}+\frac{12EI_3}{L_3^3} & \frac{-6EI_2}{L_2^2}+\frac{6EI_3}{L_3^2} & \frac{-12EI_3}{L_3^3} & \frac{6EI_3}{L_3^2} & 0 & 0\\
0 & 0 & \frac{6EI_2}{L_2^2} & \frac{2EI_2}{L_2} & \frac{-6EI_2}{L_2^2}+\frac{6EI_3}{L_3^2} & \frac{4EI_2}{L_2}+\frac{4EI_3}{L_3} & \frac{-6EI_3}{L_3^2} & \frac{2EI_3}{L_3} & 0 & 0\\
0 & 0 & 0 & 0 & \frac{-12EI_3}{L_3^3} & \frac{-6EI_3}{L_3^2} & \frac{12EI_3}{L_3^3}+\frac{12EI_4}{L_4^3} & \frac{-6EI_3}{L_3^2}+\frac{6EI_4}{L_4^2} & \frac{-12EI_4}{L_4^3} & \frac{6EI_4}{L_4^2}\\
0 & 0 & 0 & 0 & \frac{6EI_3}{L_3^2} & \frac{2EI_3}{L_3} & \frac{-6EI_3}{L_3^2}+\frac{6EI_4}{L_4^2} & \frac{4EI_3}{L_3}+\frac{4EI_4}{L_4} & \frac{-6EI_4}{L_4^2} & \frac{2EI_4}{L_4}\\
0 & 0 & 0 & 0 & 0 & 0 & \frac{-12EI_4}{L_4^3} & \frac{-6EI_4}{L_4^2} & \frac{12EI_4}{L_4^3} & \frac{-6EI_4}{L_4^2}\\
0 & 0 & 0 & 0 & 0 & 0 & \frac{6EI_4}{L_4^2} & \frac{2EI_4}{L_4} & \frac{-6EI_4}{L_4^2} & \frac{4EI_4}{L_4}
\end{bmatrix}$$

Fig. 35. Element Stiffness Matrix and Element Mass Matrix Forms of the AFL Model

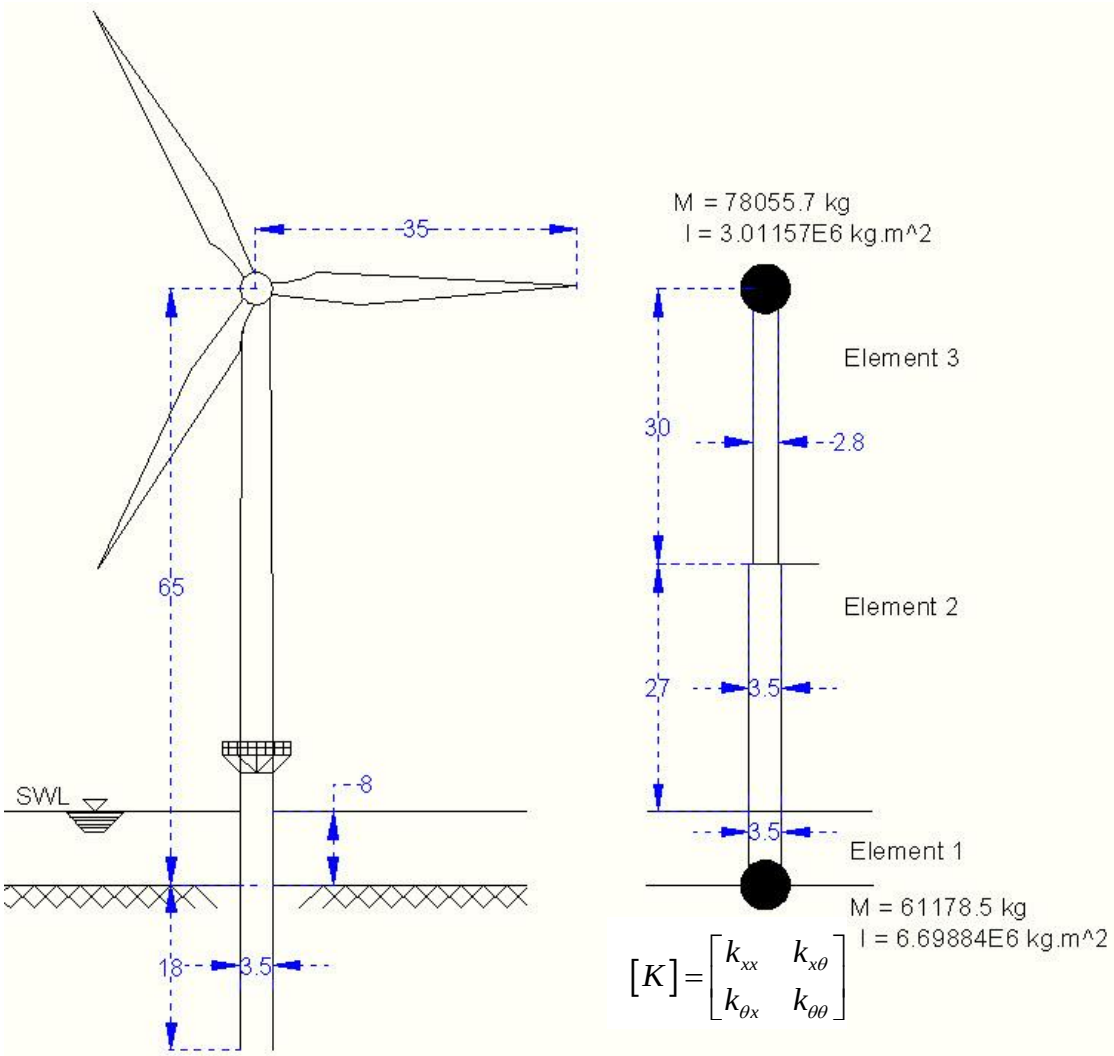

Fig. 36. Dimensions and Elements of Monopile Offshore Wind Turbine Structure (1.5 MW) Unit for the Randolph Model

$$[M]=\begin{bmatrix}
\frac{13\rho_1A_1L_1}{35}+M & \frac{11\rho_1A_1L_1^2}{210} & \frac{54\rho_1A_1L_1}{420} & \frac{-13\rho_1A_1L_1^2}{420} & 0 & 0 & 0 & 0\\
\frac{11\rho_1A_1L_1^2}{210} & \frac{\rho_1A_1L_1^3}{105}+I & \frac{13\rho_1A_1L_1^2}{420} & \frac{-3\rho_1A_1L_1^3}{420} & 0 & 0 & 0 & 0\\
\frac{54\rho_1A_1L_1}{420} & \frac{13\rho_1A_1L_1^2}{420} & \frac{13\left(\rho_1A_1L_1+\rho_2A_2L_2\right)}{35} & \frac{11\left(\rho_2A_2L_2^2-\rho_1A_1L_1^2\right)}{210} & \frac{54\rho_2A_2L_2}{420} & \frac{-13\rho_2A_2L_2^2}{420} & 0 & 0\\
\frac{-13\rho_1A_1L_1^2}{420} & \frac{-3\rho_1A_1L_1^3}{420} & \frac{11\left(\rho_2A_2L_2^2-\rho_1A_1L_1^2\right)}{210} & \frac{\left(\rho_1A_1L_1^3+\rho_2A_2L_2^3\right)}{105} & \frac{13\rho_2A_2L_2^2}{420} & \frac{-3\rho_2A_2L_2^3}{420} & 0 & 0\\
0 & 0 & \frac{54\rho_2A_2L_2}{420} & \frac{13\rho_2A_2L_2^2}{420} & \frac{13\left(\rho_2A_2L_2+\rho_3A_3L_3\right)}{35} & \frac{11\left(\rho_3A_3L_3^2-\rho_2A_2L_2^2\right)}{210} & \frac{54\rho_3A_3L_3}{420} & \frac{-13\rho_3A_3L_3^2}{420}\\
0 & 0 & \frac{-13\rho_2A_2L_2^2}{420} & \frac{-3\rho_2A_2L_2^3}{420} & \frac{11\left(\rho_3A_3L_3^2-\rho_2A_2L_2^2\right)}{210} & \frac{\left(\rho_2A_2L_2^3+\rho_3A_3L_3^3\right)}{105} & \frac{13\rho_3A_3L_3^2}{420} & \frac{-3\rho_3A_3L_3^3}{420}\\
0 & 0 & 0 & 0 & \frac{54\rho_3A_3L_3}{420} & \frac{13\rho_3A_3L_3^2}{420} & \frac{13\rho_3A_3L_3}{35}+M & \frac{-11\rho_3A_3L_3^2}{210}\\
0 & 0 & 0 & 0 & \frac{-13\rho_3A_3L_3^2}{420} & \frac{-3\rho_3A_3L_3^3}{420} & \frac{-11\rho_3A_3L_3^2}{210} & \frac{\rho_3A_3L_3^3}{105}+I
\end{bmatrix}$$

$$[K]=\begin{bmatrix}
\frac{12EI_1}{L_1^3}+k_{xx} & \frac{6EI_1}{L_1^2}+k_{x\theta} & \frac{-12EI_1}{L_1^3} & \frac{6EI_1}{L_1^2} & 0 & 0 & 0 & 0\\
\frac{6EI_1}{L_1^2}+k_{\theta x} & \frac{4EI_1}{L_1}+k_{\theta\theta} & \frac{-6EI_1}{L_1^2} & \frac{2EI_1}{L_1} & 0 & 0 & 0 & 0\\
\frac{-12EI_1}{L_1^3} & \frac{-6EI_1}{L_1^2} & \frac{12EI_1}{L_1^3}+\frac{12EI_2}{L_2^3} & \frac{-6EI_1}{L_1^2}+\frac{6EI_2}{L_2^2} & \frac{-12EI_2}{L_2^3} & \frac{6EI_2}{L_2^2} & 0 & 0\\
\frac{6EI_1}{L_1^2} & \frac{2EI_1}{L_1} & \frac{-6EI_1}{L_1^2}+\frac{6EI_2}{L_2^2} & \frac{4EI_1}{L_1}+\frac{4EI_2}{L_2} & \frac{-6EI_2}{L_2^2} & \frac{2EI_2}{L_2} & 0 & 0\\
0 & 0 & \frac{-12EI_2}{L_2^3} & \frac{-6EI_2}{L_2^2} & \frac{12EI_2}{L_2^3}+\frac{12EI_3}{L_3^3} & \frac{-6EI_2}{L_2^2}+\frac{6EI_3}{L_3^2} & \frac{-12EI_3}{L_3^3} & \frac{6EI_3}{L_3^2}\\
0 & 0 & \frac{6EI_2}{L_2^2} & \frac{2EI_2}{L_2} & \frac{-6EI_2}{L_2^2}+\frac{6EI_3}{L_3^2} & \frac{4EI_2}{L_2}+\frac{4EI_3}{L_3} & \frac{-6EI_3}{L_3^2} & \frac{2EI_3}{L_3}\\
0 & 0 & 0 & 0 & \frac{-12EI_3}{L_3^3} & \frac{-6EI_3}{L_3^2} & \frac{12EI_3}{L_3^3} & \frac{-6EI_3}{L_3^2}\\
0 & 0 & 0 & 0 & \frac{6EI_3}{L_3^2} & \frac{2EI_3}{L_3} & \frac{-6EI_3}{L_3^2} & \frac{4EI_3}{L_3}
\end{bmatrix}$$

Fig. 37. Element Stiffness Matrix and Element Mass Matrix Forms of the Randolph Model

velocity, G_S is the soil shear modulus, ρ_S is the soil mass density, and $c(a_0)$ is the dimensionless damping coefficient. The dynamic-stiffness coefficient can be interpreted as a spring $K\,k(a_0)$ and a parallel dashpot $K\frac{r_0}{c_S}c(a_0)$ for harmonic excitation (for more information, see Wolf and Deeks 2004). Based on this, the three terms, the sliding, rotation, and coupling dynamics-stiffness coefficient terms are transferred to harmonic excitation forms and are added to the stiffness matrix system. The parallel dash terms are not included in this scenario because all the scenarios for the 1.5MW capacity unit are assumed to be uniform undamped soil in order to compare the AFL, Randolph, and modified cone models. In the modified cone model, the finite element model, the element stiffness matrix, and the element mass matrix are treated in the same way as the Randolph Model, except for the pile-soil interaction behavior, the harmonic excitation form of equation (39) is used instead of equation (36) in the Randolph model. Program CONAN (CONe ANalysis) is used to estimate the dynamic-stiffness coefficients of the modified cone model (see Wolf and Deeks 2004).

The thrust force used to excite the wind tower structures used with each of the foundation models (AFL, Randolph, and modified cone) was developed using the FAST Software, (Jonkman and Buhl Jr. 2005) for the 1.5 MW capacity unit. Three different cases that were defined in the FAST documentation (Test 11, 12, and 13) were used in the response computations. The signals are depicted in Fig. 38. The difference between the signals is shown in Table 6. The first 15 seconds of the signal from the thrust time series simulations is cut because, as shown in Fig. 38, there is an unexplained transient fluctuation in the thrust force signal.

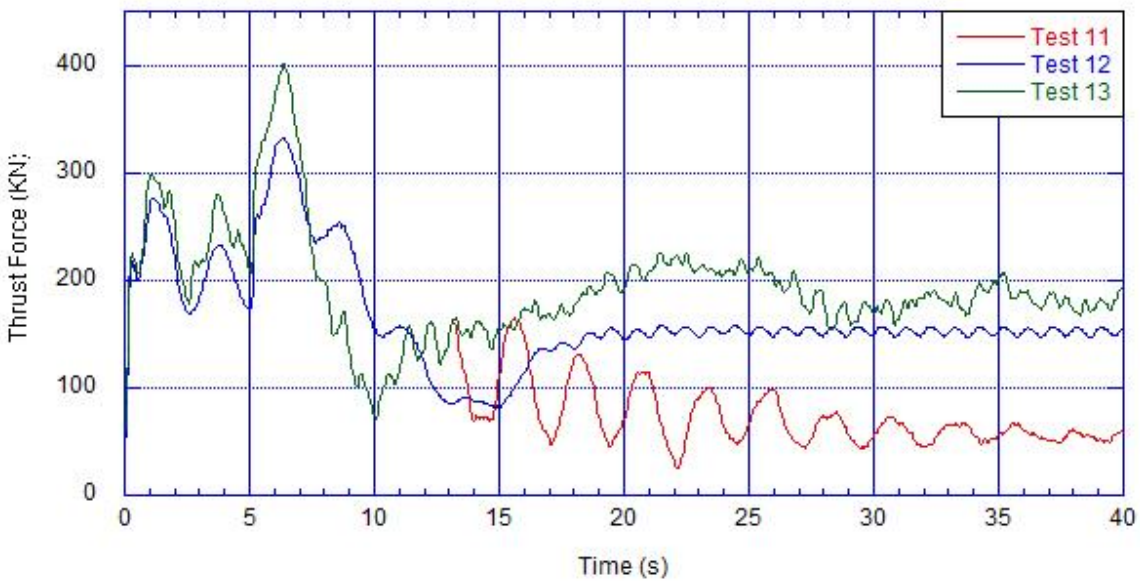

Fig. 38. Inline Thrust Force Signals Generated Using NREL's FAST Software

Table 6 Three Different Thrust Force Cases for 1.5 MW (Jonkman and Buhl Jr. 2005)

Test Name	Rotor Dia. (m)	Test Description
Test 11	70	Flexible, variable speed & pitch control, pitch failure, turbulence
Test 12	70	Flexible, variable speed & pitch control, ECD[1] event
Test 13	70	Flexible, variable speed & pitch control, turbulence

[1] Extreme Coherent Gust with Direction Change

Two scenarios were run with the three different thrust force cases (Test 11, 12, and 13) and repeated with each of the three different foundation models (AFL, Randolph, and modified cone). In the first scenario the hub height $(H_B = 65m)$ of the offshore wind turbine structure was held constant and the water depth was varied $(D = 8m, 12m, 16m, \text{ and } 20m)$. The second scenario involved fixing the water depth $(D = 8m)$ and changing the hub height elevation $(H_B = 50m, 55m, 60m, \text{ and } 65m)$. The maximum total moment $(M_{Max}, KN.m)$ with respect to the center of rotation , maximum total top horizontal displacement of the structure (δ_{Max}, m), and maximum tilt at the head of the foundation $(\alpha_{Max}, \text{deg.})$ of the two scenarios are presented in Tables 7 and 8.

Two dimensionless terms, (y/y_c) and (δ_{Max}/h_b), are investigated for the 1.5 MW Unit, based on Tables 7 and 8. Where h_b is the rotor hub height from the seabed level, y is the maximum horizontal displacement at the head of the monopile foundation, and y_c is the horizontal displacement of soil corresponding to 50% of ultimate horizontal soil resistance and can be calculated by the following equation:

$$y_c = 2.5 \times \varepsilon_{50} \times B \quad ; \quad \varepsilon_{50} = 0.007 \quad \text{for stiff clay} \tag{40}$$

where ε_{50} is the strain at 50% strength level and B is the diameter of the pile, based on Deng and Ma (2000). The dimensionless terms are depicted in Tables 9 and 10. From these tables, the (y/y_c) term has a range of 0.028 to 0.382, which means that the response is linear and the monopile foundation is not in the yielding zone. In addition, the (δ_{Max}/h_b) term has a range of 0.0029 to 0.011.

As shown in Fig. 39 and 40, the modified cone model exhibits a stiffer behavior and

Table 7 Maximum Response Behavior of a 1.5 MW Unit as a Function of Water Depth for Three NREL Operational Load Scenarios

Water Depth	Case	AFL			Randolph			Modified Cone Model		
		M_{Max} KN.m	α_{Max} deg	δ_{Max} m	M_{Max} KN.m	α_{Max} deg	δ_{Max} m	M_{Max} KN.m	α_{Max} deg	δ_{Max} m
8*m*	11	13105	0.1680	0.6510	12850	0.1401	0.6365	13980	0.0147	0.4036
	12	12543	0.1082	0.3968	12307	0.0874	0.3652	13397	0.0104	0.2575
	13	17419	0.1521	0.5746	17084	0.1245	0.5360	18584	0.0149	0.3955
12*m*	11	13649	0.1750	0.6654	13397	0.1448	0.6403	14524	0.0159	0.3996
	12	13087	0.1215	0.4290	12852	0.0979	0.3930	13938	0.0116	0.2704
	13	17965	0.1651	0.6048	17631	0.1350	0.5618	19128	0.0161	0.4072
16*m*	11	14237	0.1828	0.6854	13994	0.1517	0.6495	15106	0.0172	0.4173
	12	13673	0.1369	0.4716	13438	0.1103	0.4304	14518	0.0130	0.2898
	13	18552	0.1800	0.6437	18219	0.1471	0.5960	19710	0.0174	0.4249
20*m*	11	14854	0.1922	0.7099	14610	0.1634	0.6700	15715	0.0187	0.4415
	12	14287	0.1546	0.5245	14054	0.1245	0.4779	15124	0.0145	0.3170
	13	19167	0.1968	0.6929	18834	0.1608	0.6399	20319	0.0189	0.4501

Note: 65m Hub Height

Table 8 Maximum Response Behavior of a 1.5 MW Unit as a Function of Hub Height for Three NREL Operational Load Scenarios

Hub Height	Case	AFL			Randolph			Modified Cone Model		
		M_{Max} KN.m	α_{Max} deg	δ_{Max} m	M_{Max} KN.m	α_{Max} deg	δ_{Max} m	M_{Max} KN.m	α_{Max} deg	δ_{Max} m
50*m*	11	10461	0.1177	0.3347	10220	0.0961	0.3098	11343	0.0117	0.2263
	12	10014	0.0825	0.2243	9787	0.0661	0.2047	10885	0.0081	0.1427
	13	13873	0.1183	0.3367	13547	0.0964	0.3116	15058	0.0118	0.2272
55*m*	11	11340	0.1279	0.3976	11095	0.1046	0.3700	12214	0.0127	0.2717
	12	10852	0.0906	0.2719	10621	0.0729	0.2489	11715	0.0088	0.1735
	13	15050	0.1295	0.4042	14721	0.1055	0.3747	16229	0.0128	0.2731
60*m*	11	12211	0.1445	0.5231	11975	0.1128	0.4688	13098	0.0137	0.3257
	12	11695	0.0992	0.3289	11462	0.0800	0.3018	12551	0.0096	0.2114
	13	16232	0.1409	0.4834	15899	0.1150	0.4493	17404	0.0138	0.3287
65*m*	11	13105	0.1680	0.6510	12850	0.1401	0.6365	13980	0.0147	0.4036
	12	12543	0.1082	0.3968	12307	0.0874	0.3652	13397	0.0104	0.2575
	13	17419	0.1521	0.5746	17084	0.1245	0.5360	18584	0.0149	0.3955

Note: 8m Water Depth

Table 9 Two Dimensionless Terms of a 1.5 MW Unit as a Function of Water Depth for Three NREL Operational Load Scenarios

Water Depth	Case	AFL		Randolph		Modified Cone Model	
		y/y_c	δ_{Max}/h_b	y/y_c	δ_{Max}/h_b	y/y_c	δ_{Max}/h_b
8*m*	11	0.325	0.01	0.212	0.0098	0.049	0.0062
	12	0.211	0.006	0.136	0.0056	0.036	0.004
	13	0.296	0.009	0.191	0.008	0.051	0.006
12*m*	11	0.338	0.01	0.22	0.0099	0.054	0.006
	12	0.237	0.0066	0.152	0.006	0.039	0.004
	13	0.32	0.0093	0.207	0.0086	0.054	0.0063
16*m*	11	0.353	0.0105	0.232	0.01	0.057	0.0064
	12	0.266	0.0073	0.17	0.0066	0.044	0.0045
	13	0.35	0.0099	0.225	0.0092	0.059	0.0065
20*m*	11	0.371	0.011	0.25	0.0103	0.062	0.0068
	12	0.3	0.0081	0.193	0.0074	0.049	0.0049
	13	0.382	0.011	0.247	0.0098	0.064	0.0069

Note: 65m Hub Height

Table 10 Two Dimensionless Terms of a 1.5 MW Unit as a Function of Hub Height for Three NREL Operational Load Scenarios

Hub Height	Case	AFL		Randolph		Modified Cone Model	
		y/y_c	δ_{Max}/h_b	y/y_c	δ_{Max}/h_b	y/y_c	δ_{Max}/h_b
50*m*	11	0.23	0.0067	0.15	0.0062	0.039	0.0045
	12	0.163	0.0045	0.104	0.0041	0.028	0.0029
	13	0.232	0.0067	0.15	0.0062	0.041	0.0045
55*m*	11	0.25	0.0072	0.162	0.0067	0.042	0.0049
	12	0.178	0.0049	0.114	0.0045	0.031	0.0032
	13	0.253	0.0073	0.163	0.0068	0.044	0.005
60*m*	11	0.279	0.0087	0.173	0.0078	0.046	0.0054
	12	0.194	0.0055	0.124	0.005	0.033	0.0035
	13	0.274	0.008	0.176	0.0075	0.046	0.0055
65*m*	11	0.325	0.01	0.212	0.0098	0.049	0.0062
	12	0.211	0.006	0.136	0.0056	0.036	0.004
	13	0.296	0.0088	0.191	0.0082	0.051	0.006

Note: 8m Water Depth

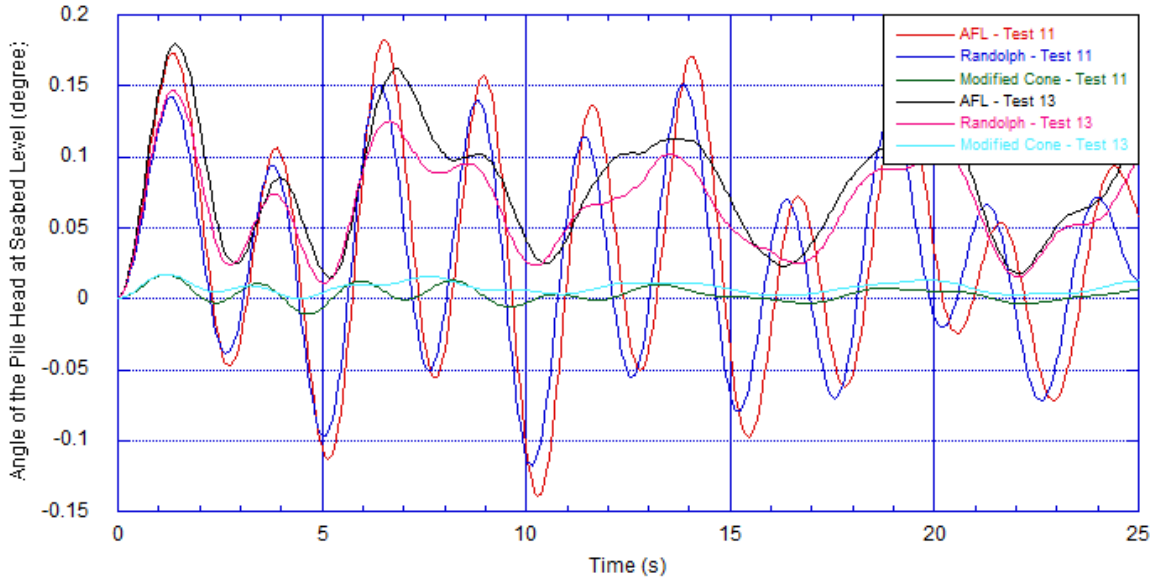

Fig. 39. Pile Head Angle Results of 1.5 MW Unit with Water Depth $(D=16m)$ and Hub Height $(H_B=65m)$

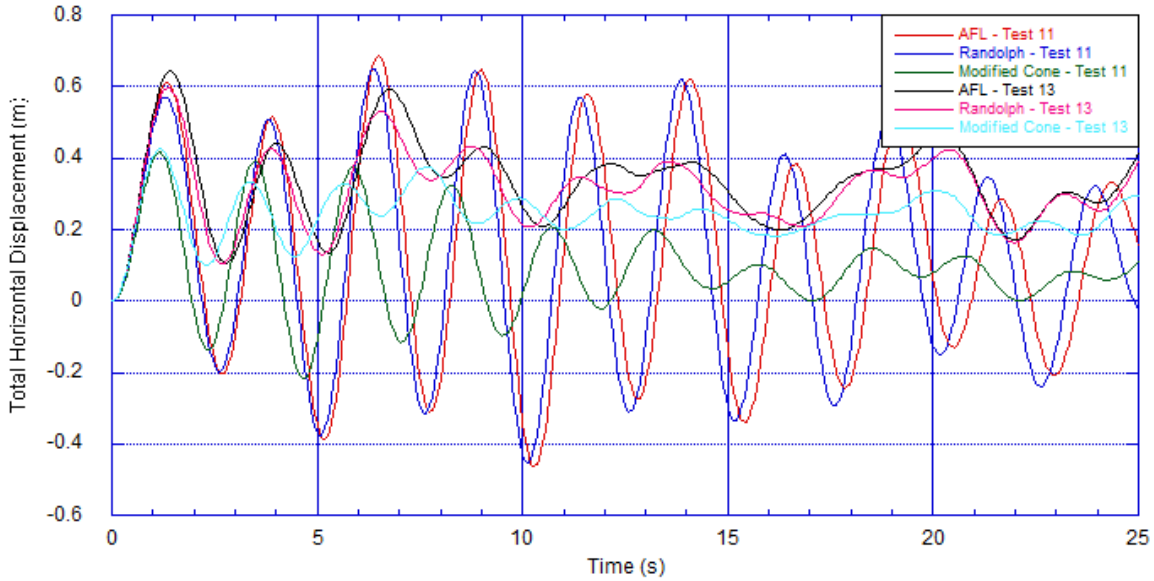

Fig. 40. Horizontal Displacement Results of 1.5 MW Unit with Water Depth $(D=16m)$ and Hub Height $(H_B=65m)$

experiencing less effects for the case of blade pitch failure when compared with the apparent fixity level and Randolph models. In addition, the apparent fixity level and Randolph models are in phase for both thrust force cases (Test 11 and Test 13). However, the Randolph foundation model is a little bit stiffer than apparent fixity level model, specifically for a modulus of elasticity of $80MN/m^2$ used in the Randolph model, and choosing $3.7D$ for the apparent fixity level based upon a $3.5m$ diameter for the 1.5 MW unit. The apparent fixity level model is easy to apply and appears to be more conservative, according to the results from Fig. 39 and 40. In general, the angle of the pile head at seabed level in Fig. 39 is small, and the total horizontal displacement is less but it is the same order of magnitude in Fig. 40, which reflects the flexibility of the top tower.

4.3 Modified Cone Model (3.0 MW) Unit

Wolf and Meek (1994) extended the cone models to represent an embedded foundation, such as the monopile, suction caisson, and gravity-based foundations in a multiple-layered half-space. Then using the modified cone model one can estimate the dynamic-stiffness coefficients for each of the three different foundation types for the 3.0 MW capacity unit. The modified cone model is used to obtain a more in depth understanding of the behavior (sliding and rotation) of the offshore wind turbine structure with different types of foundations. The modified cone model was used in the numerical simulations to estimate the maximum total moment with respect to the center of rotation, the maximum total top horizontal displacement of the structure, and the maximum tilt at the head of the foundation for the offshore wind turbine 3.0 MW unit for each of the foundation types. As previously mentioned, two different soil conditions are used in this

model for each type of foundation: one uniform layer of stiff clay and the three different soil layers with the soil properties presented in Fig. 33.

The two main scenarios for the modified cone model were run with two different soil conditions for each foundation system. Each one of these scenarios involved fixing the hub height elevation $\left(H_B = 80m\right)$ of the offshore wind turbine structure and changing the water depth $\left(D = 8m, 12m, 16m, and\ 20m\right)$. Then, the water depth was fixed $\left(D = 10m\right)$ and only the hub height elevation was changed $\left(H_B = 60m, 65m, 70m, 75m, and\ 80m\right)$. The idea behind changing the water depth and the hub height was to obtain a better understanding of the offshore wind turbine's overall structural response behavior. The maximum total moment $\left(M_{Max}, KN.m\right)$ with respect to the center of rotation, maximum total top horizontal displacement of the structure $\left(\delta_{Max}, m\right)$, and maximum tilt at the head of the foundation $\left(\alpha_{Max}, \deg.\right)$ was calculated and the numerical results are presented in Tables 11, 12, 13, and 14.

Based on the single-layer modified cone model (Tables 11 and 12), the average reduction of δ and α are estimated for suction caisson and gravity-based foundations with respect to the monopile foundation. The suction caisson and gravity-based foundation models have an average of 12% reduction of δ compared with the monopile foundation model. In addition, the suction caisson and gravity-based foundation models have an average of 62% and 58% reductions of α, respectively, which means that the monopile foundation model has the highest amount of flexible behavior compared with the suction caisson and gravity-based foundation models. However, for the three-layer modified cone model (Tables 13 and 14), the suction caisson and gravity-based

Table 11 Maximum Response Behavior of a 3.0 MW Unit as a Function of Water Depth Based Upon a Single Layer Modified Cone Model

Water Depth	Monopile			Suction Caisson			Gravity Based		
	M_{Max} KN.m	α_{Max} deg	δ_{Max} m	M_{Max} KN.m	α_{Max} deg	δ_{Max} m	M_{Max} KN.m	α_{Max} deg	δ_{Max} m
8*m*	13265	0.0369	0.3686	12700	0.0141	0.3284	11984	0.0155	0.3285
12*m*	13804	0.0402	0.3830	13248	0.0153	0.3379	12538	0.0168	0.3379
16*m*	14377	0.0440	0.4026	13826	0.0167	0.3522	13119	0.0183	0.3524
20*m*	14978	0.0481	0.4283	14425	0.0183	0.3719	13721	0.0201	0.3722

Note: 80m Hub Height

Table 12 Maximum Response Behavior of a 3.0 MW Unit as a Function of Hub Height Based Upon a Single Layer Modified Cone Model

Hub Height	Monopile			Suction Caisson			Gravity Based		
	M_{Max} KN.m	α_{Max} deg	δ_{Max} m	M_{Max} KN.m	α_{Max} deg	δ_{Max} m	M_{Max} KN.m	α_{Max} deg	δ_{Max} m
60*m*	10788	0.0312	0.2294	10278	0.0115	0.2018	9622	0.0124	0.2014
65*m*	11467	0.0331	0.2588	10938	0.0123	0.2282	10269	0.0133	0.2278
70*m*	12146	0.0350	0.2929	11609	0.0131	0.2583	10925	0.0143	0.2581
75*m*	12835	0.0368	0.3315	12286	0.0139	0.2931	11588	0.0152	0.2930
80*m*	13529	0.0385	0.3752	12969	0.0147	0.3326	12257	0.0161	0.3327

Note: 10m Water Depth

Table 13 Maximum Response Behavior of a 3.0 MW Unit as a Function of Water Depth Based Upon a Three Layer Modified Cone Model

Water Depth	Monopile			Suction Caisson			Gravity Based		
	M_{Max} KN.m	α_{Max} deg	δ_{Max} m	M_{Max} KN.m	α_{Max} deg	δ_{Max} m	M_{Max} KN.m	α_{Max} deg	δ_{Max} m
8*m*	12639	0.0161	0.3315	12665	0.0041	0.3129	12085	0.0062	0.3153
12*m*	13184	0.0175	0.3413	13217	0.0045	0.3206	12642	0.0067	0.3235
16*m*	13761	0.0191	0.3562	13794	0.0049	0.3330	13222	0.0073	0.3362
20*m*	14363	0.0209	0.3762	14389	0.0053	0.3502	13820	0.0080	0.3537

Note: 80m Hub Height

Table 14 Maximum Response Behavior of a 3.0 MW Unit as a Function of Hub Height Based Upon a Three Layer Modified Cone Model

Hub Height	Monopile			Suction Caisson			Gravity Based		
	M_{Max}	α_{Max}	δ_{Max}	M_{Max}	α_{Max}	δ_{Max}	M_{Max}	α_{Max}	δ_{Max}
60m	10197	0.0132	0.2040	10289	0.0033	0.1919	9755	0.0049	0.1934
65m	10865	0.0141	0.2305	10935	0.0036	0.2166	10392	0.0053	0.2182
70m	11539	0.0150	0.2611	11593	0.0038	0.2455	11038	0.0057	0.2475
75m	12221	0.0159	0.2960	12262	0.0040	0.2785	11695	0.0060	0.2809
80m	12906	0.0167	0.3359	12938	0.0043	0.3162	12360	0.0064	0.3189

Note: 10m Water Depth

foundation models have 6.3% and 5.4% average reduction of δ, respectively, and an average of 74.5% and 61.7% reductions of α, respectively.

As previously mentioned, a replicated in-line thrust force signal was used in the numerical simulation (Wolf and Deeks 2004). In Fig. 41 the replicated thrust force signal of the two-bladed 3.0 MW unit is compared with the three case signals obtained from the FAST Software for the three-bladed 1.5 MW unit. Each of the signals were virtually the same wind velocity of 13 m/s. As shown in Fig. 41, the three-bladed (1.5 MW) unit has more thrust force than the two-bladed (3.0 MW) unit, except during test 13, which demonstrates pitch failure of one of the blades on the three-bladed (1.5 MW) after 13 seconds. Morison's equation is used for all scenarios, and the drag force modeling equation is used for estimating the aerodynamic loading on the slender tower. Lastly, FNV is used in one of the previous scenarios and is shown in Table 15 . Based on the numbers of the figure, FNV method appears to generate less wave force than Morison's equation in this type of situation.

As shown in Fig. 42 and 43, the suction caisson model shows more stiff behavior than the gravity-based and monopile models. With respect to the soil condition, the monopile model has the highest flexible behavior as comparing with the suction caisson and gravity-based models. Relatively, the gravity-based model has very close results comparing with the suction caisson model. The angle of the foundation head at seabed level in Fig. 42 is pretty much in phase. In Fig. 43, the monopile soft clay case has the largest displacement, which is consistent with Fig. 42 on angle. The monopile soft soil case begins slightly out of phase and becomes more so as time progresses. All cases in Fig. 43 demonstrate a damping of the displacement, and the steady state appears to be a

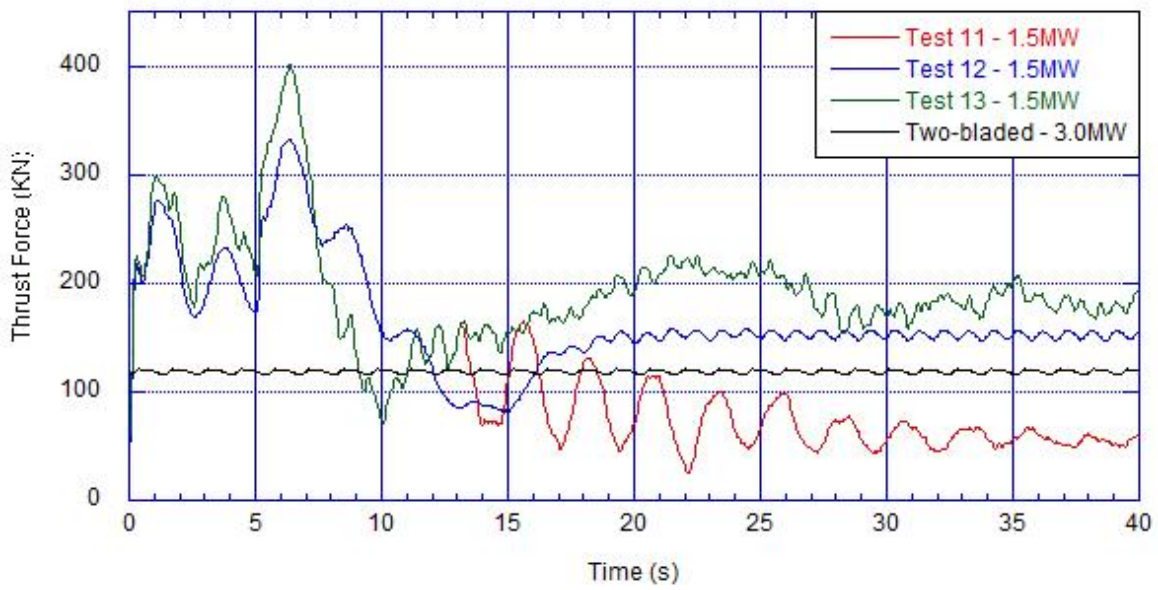

Fig. 41. Thrust Force Signals of Two-Bladed (3.0 MW) and Three-Bladed (1.5MW) Units

Table 15 Maximum Response Behavior of a 3.0 MW Unit as a Function of Water Depth Based Upon a Three Layer Modified Cone Model and FNV Theory

Water Depth	Monopile			Suction Caisson			Gravity Based		
	M_{Max} KN.m	α_{Max} deg	δ_{Max} m	M_{Max} KN.m	α_{Max} deg	δ_{Max} m	M_{Max} KN.m	α_{Max} deg	δ_{Max} m
8*m*	12131	0.0138	0.3296	12064	0.0036	0.3119	11466	0.0056	0.3143
12*m*	12576	0.0141	0.3352	12508	0.0037	0.3167	11912	0.0057	0.3193
16*m*	13161	0.0145	0.3427	13089	0.0038	0.3234	12497	0.0059	0.3262
20*m*	13832	0.0150	0.3524	13756	0.0039	0.3319	13167	0.0061	0.3350

Note: 80m Hub Height

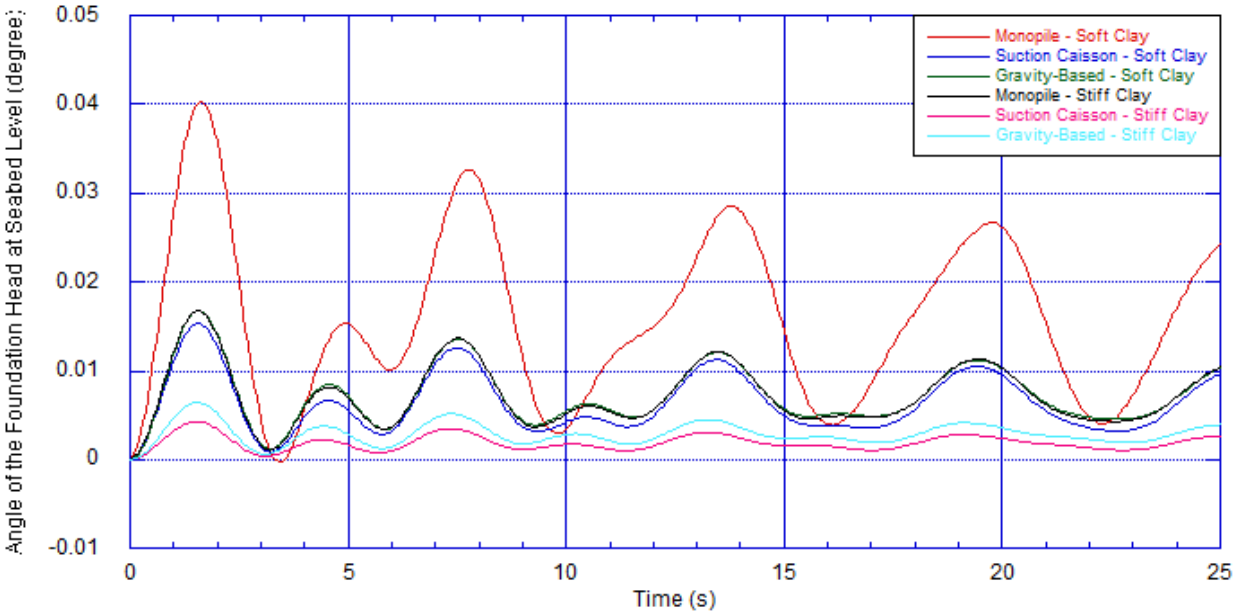

Fig. 42. Pile Head Angle Results of 3.0 MW Unit with Water Depth $(D=12m)$ and Hub Height $(H_B=80m)$

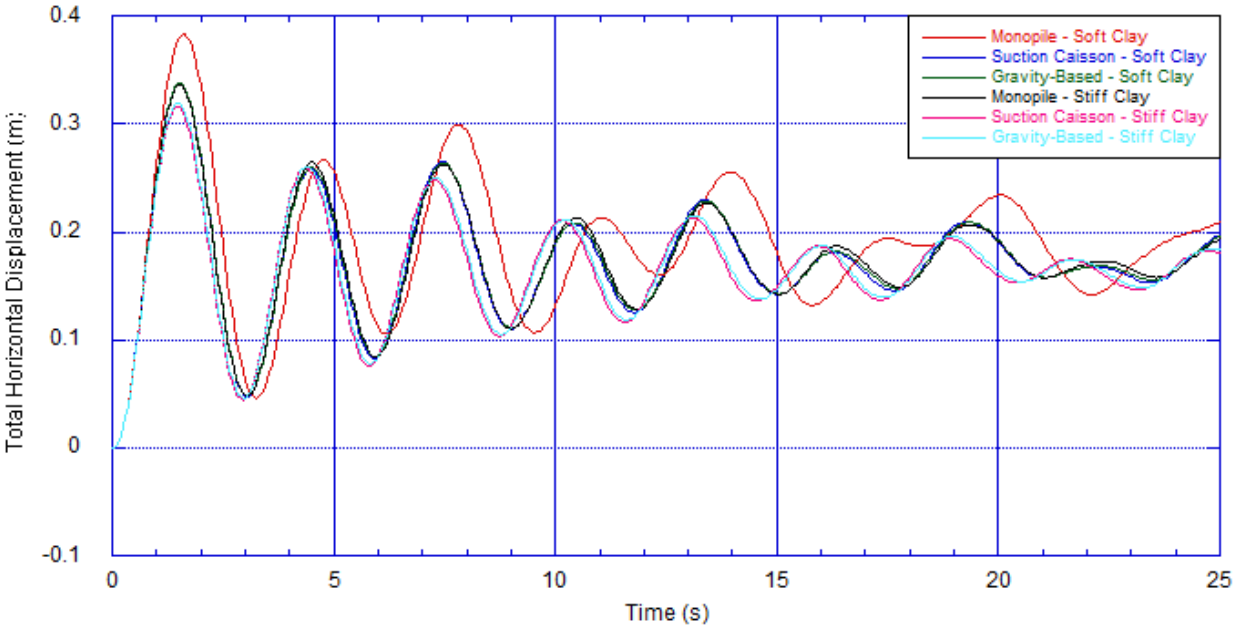

Fig. 43. Horizontal Displacement Results of 3.0 MW Unit with Water Depth $(D=12m)$ and Hub Height $(H_B=80m)$

total displacement value in the range of 0.18 - 0.2 m. The dimensionless term (y/y_c) for both cases (one and three layer modified cone models) has linear response and the monopile foundation is not in the yielding zone.

5. SUMMARY AND CONCLUSION

As countries worldwide pursue their stated goals to become less dependent on non-renewable sources of energy, the potential of the natural wind resource available to those countries having access to offshore sites presents an attractive option. Several innovative offshore concepts were presented that illustrate the parallel development with earlier offshore and gas platform concepts but have a distinctively different objective. The magnitude of this resource, which is the driving force for these innovations, was briefly presented in the introduction. The discussion included a selective overview of the increasing number offshore farms that have been developed or are planned. Moving land-based technology to the offshore presents many technical challenges within the broad range of topics including design, manufacturing, installation, operation, maintenance and removal. This research study was focused upon modeling of a single offshore wind tower with an emphasis of developing a basic finite element model that better addressed several typical foundation types, the local soil variability, and an alternative wave force model in the time domain. The offshore industry has used single pile, gravity base and suction caissons foundations for their various platform and anchoring system designs. This research study highlighted examples most relevant to offshore wind turbines and illustrated the use of time dependent wind thrust output from NREL's FAST software as input to the dynamic response of the basic finite element model presented in this study. The emphasis was on developing a basic model of a single wind turbine tower that would capture the various considerations without being too simple or overwhelming.

A series of numerical examples were investigated in order to examine several key design parameters for a monopile wind turbine tower. The parameters of particular

concern were the bending moment at the seafloor elevation, the off vertical angular rotation of the tower at the seabed and the horizontal deflection at the hub elevation. Manufactures have strict limits on the rotation angle and hub elevation deflection as the blades for upwind wind turbines are often long and flexible and the chance for blade tower impacts must be avoided.

According to the maximum response behavior, the off vertical angular rotation of the tower at the seabed and the horizontal deflection at the hub elevation, of a 1.5 MW unit, the modified cone model shows stiffer behavior and less effect on the blade pitch failure compared with the apparent fixity level and the Randolph elastic continuum models. For all models, the effect of the blade pitch failure (Test 11) on the offshore wind turbine structure decreases with increasing water depth, and increases with increasing hub height of the structure. From the result, the apparent fixity level model is a little bit more flexible than the Randolph model, based on choosing $3.7D$ as an effective depth of the pile below the seabed, and choosing a modulus of elasticity equal to $80MN/m^2$ for the Randolph model, where D is the diameter of the pile and is equal to $3.5m$ in the 1.5MW unit.

In addition to these findings, the maximum response behavior of the vertical angular rotation of the foundation head at seafloor and the horizontal displacement of a 3.0 MW unit show that the suction caisson model has more stiff behavior than gravity-based and monopile models. Moreover, the monopile model has the highest amount of flexible behavior as compared with the suction caisson and the gravity-based models with respect to the soil condition. Relatively, the behavior of the gravity-based model does not differ very much when compared with behavior of the suction caisson model. Finally, the results show that the response behavior of a 3.0 MW unit with the nonlinear wave force

model (FNV-Theory) has less wave force when compared with the linear form of Morison's equation in these types of parametric conditions.

There is a need for more simulations and more field data to improve the simulation accuracy of the offshore wind turbine structural designs. In this research study, the results show that the flexibility of the offshore wind turbine tower is key to the total horizontal displacement of the structure. They also show that the soil properties of the foundation controls the angle of the foundation head at seabed level. The varying soil properties across foundation models will change the behavior of the structure; therefore, the modified cone foundation model should be used. The apparent fixity level is easy to apply, and it can predict the behavior of the structure, as it appears to be more conservative and a good choice for first pass. However, to further refine the behavior of the structure, the horizontal displacement at the top of the structure, the angle of the foundation head at seabed level, and the multi-layered damping soil system, the modified cone model is the best option for counting those variables, since it is not possible to include the multi-layered damping soil system in the apparent fixity level and Randolph models.

REFERENCES

Architecture News, World Architects, Buildings, Photos, Architectural Developments. Strata Tower, London : Elephant & Castle Building 2010. (http://www.e-architect.co.uk)

Barthelmie, R. J., Larsen, G. C., Pryor, S. C., Jorgensen, H., Bergstrom, H., Schlez, W., Rados, K., Lange, B., Vølund, P., Neckelmann, S., Mogensen, S., Schepers, J. G., Hegberg, T., Folkerts, L. and Magnusson, M. 2004. "ENDOW (Efficient Development of Offshore Wind Farms): Modelling Wake and Boundary Layer Interactions Article", Wind Energy, 7, 225-245.

Businessweek is a weekly business magazine published by Bloomberg L.P. Innovative Wind Turbine Design Triples Output 2009. (http://www.businessweek.com)

Byrne, B. W. and Houlsby, G. T. 2003. Foundation for offshore wind turbines, Phil. Trans. Of the Royal Society of London, Series A 361, 2909-2300.

Byrne, B. W. and Houlsby, G. T. 2000. Suction caisson foundations for offshore wind turbines and anemometer masts. Wind Engineering 24 (4), 249-255.

Clough, R. W. and Penzien, J. 1975. Dynamics of Structures, McGraw-Hill, New York.

Deng, N. and Ma, Y. 2000. "Deep Foundations" Bridge Engineering Handbook, CRC Press, Boca Raton, 2020 p.

DNV-RP-C205 2007. Environmental Conditions and Environmental Loads, Det Norske Veritas, Norway, 122 p.

Elliott, D. and Schwartz, M. 2006. Wind Resource Mapping for United States Offshore Areas, NREL/CP-500-40045, WindPower Conference Pittsburgh, Pennsylvania, June 4-7.

Faltinsen, O. M., Newman, J. N. and Vinje, T. 1995. Nonlinear Wave Loads on a Slender Vertical Cylinder, J. Fluid Mech. 289, 179-198.

Ferguson, M., Kühn, M., Bierbooms, W., Cockerill, T., Göransson, B., Harland, L., van Bussel, G., Vugts, J. and Hes R. 1998. Opti-OWECS Final Report Vol. 4: A Typical Design Solution for an Offshore Wind Energy Conversion System, Institute for Wind Energy, Delft University of Technology, Delft.

Frandsen, S. 1992. On the wind speed reduction in the center of large clusters of wind turbines, Journal of Wind Engineering and Industrial Aerodynamics 39, 251-265.

Frandsen, S. T. and Thøgersen, M. L. 1999. Integrated Fatigue Loading for Wind Turbine in Wind Farms by Combining Ambient Turbulence and Wakes. Wind Engineering 23 (6), 327-339.

Gipe, P. 2004. WIND POWER: Renewable Energy for Home, Farm, and Business. White River Junction, VT, Chelsea Green Pub. Co., 496p.

Gizmag is a technology weblog covers invention, innovation and emerging technologies in all fields of human endeavour. Energy-Positive Wind Powered Rotating Skyscraper Set to Begin Construction in Dubai 2008. (http://www.gizmag.com)

Gizmodo is a technology weblog about consumer electronics. The Most Powerful Wind Turbine Looks Like the Weirdest Too 2010. (http://www.gizmodo.com)

Hallam, M. G., Heaf, N. J. and Wootton, L. R. 1978. Dynamics of Marine Structures: Methods of Calculating the Dynamic Response of Fixed Structures Subject to Wave and Current action. CIRIA Underwater Engineering Group, Report UR8.

Hau, E. 2005. Wind Turbines: Fundamentals, Technologies, Applications, Economics, 2nd edition, Springer, New York, 783p.

Hexicon is a Swedish Renewable Energy Corporation. Hexicon Offshore Concept 2010. (http://www.hexicon.eu)

IEC 61400-1 2005 Wind Turbines, Part 1: Design Requirements, International Electrotechnical Committee, 3rd edition, 90 p.

Inhabitat is a weblog devoted to the future of design, tracking the innovations in technology towards a smarter and more sustainable future. Turbine Light Illuminates Highways with Wind 2010. (http://www.inhabitat.com)

Jensen, N. O. 1983. A note on wind generator interaction, Risø-M-2411, Risø National Laboratory, Denmark.

Jonkman, J. M. and Buhl Jr., M. L. 2005. FAST User's Guide, Rep. No. NREL/TP-500-38230, NREL, Golden, Colorado, USA.

Kühn, M., Cockerill, T., Harland, L., Harrison, R., Schontag, C., van Bussel, G., and Vugts, J. 1998. Opti-OWECS Final Report Vol. 2: Method Assisting the Design of Offshore Wind Energy Conversion Systems, Institute for Wind Energy, Delft University of Technology, Delft.

Kwon, Y. W. and Bang, H. 2000. The Finite Element Method Using MATLAB, 2nd edition, CRC Press, Boca Raton, 624 p.

Lavassas, I., Nikolaidis, G., Zervas, P., Efthimiou, E., Doudoumis, I.N., and Baniotopoulos, C.C. 2003. Analysis and design of the prototype of a steel 1-MW wind turbine tower, Engineering Structures 25, 1097-1106.

Magnusson, M. and Smedman, A. S. 1996. A Practical Method to Estimate Wind Turbine Wake Characteristics from Turbine Data and Routine Wind Measurements, Wind Engineering 20 (2), 73-91.

Merz, K. O., Moe, G. and Gudmestad, O. T. 2009 "A Review of Hydrodynamic Effects on Bottom-Fixed Offshore Wind Turbines," OMAE 2009, pp15.

Morison, J. R., O'Brien, M. P., Johnson, J. W., and Schaaf, S. A. 1950. The Forces Exerted by Surface Waves on Piles. Petroleum Trans., AIME 189, 149-157.

Morris, M. J., Camp, T. R., Rooij, R., Tempel, J. Zaaijer, M., Henderson, A., Argyriadis, K., Schwartz, S., Just, H., Grainger, W. and Pearce, D. 2003. Design Methods for Offshore Wind Turbines at Exposed Sites, EU Joule III Project JOR3-CT95-0284, Final Report No. 2317/BR/22D, Bristol, UK.

Morsetti, G., Poloni, C., and Diviacco, B. 1994. Optimization of Wind Turbine Positioning in Large Windfarms by Means of a Genetic Algorithm, Journal of Wind Engineering and Industrial Areodynamics 51, 105-116.

Musial, W. and Ram, B. 2010. Large-Scale Offshore Wind Power in the United States ASSESSMENT OF OPPORTUNITIES AND BARRIERS, Rep. No. NREL/TP-500-40745, NREL, Golden, Colorado, USA.

Nataraja, R. and Kirk, C. L. 1977. Dynamic Response of a Gravity Platform under Random Wave Forces, Proceedings of the Offshore Technology Conference, Paper OTC-2904.

Newmark, N. M. 1959. A Method of Computation for Structural Dynamics, Journal of Engineering Mechanics Division, ASCE 85 (ST3), 67-94.

Paz, M. 1997. Structural Dynamics Theory and Computation, 4th edition. Speed Scientific School University of Louisville. Louisville, KY, 825 p.

Randolph, M. F. 1981. The Response of Flexible Piles to Lateral Loading, Geotechnique 31 (2), 247-259.

Ransom, D. L. and Moore, J. Going Green: SwRI Engineers Design, Build and Test a Prototype Wind Turbine Array. Southwest Research Institute, Summer 2009 Technology Today, San Antonio, Texas.

Spera, D. A. 1994. Wind Turbine Technology: Fundamental Concepts of Wind Turbine Engineering. American Society of Mechanical Engineers, New York, 638p.

Statoil is a Norwegian oil and gas company 2009. (http://www.statoil.com)

Tempel, J. Van Der 2006. Design of Support Structures for Offshore Wind Turbines. PhD dissertation, Delft University of Technology, Delft.

The Times is a daily national newspaper published in the United Kingdom since 1785. Architech David Fisher Designs First Rotating Skyscraper for Dubai and Moscow 2008. (http://www.thetimes.co.uk)

Twidell, J. and Gaudiosi G. 2009. Offshore Wind Power. Brentwood, Essex CM15 9TB, United Kingdom.

US Army Corps of Engineers (USACE) 2004. Hydrodynamic Effects on Offshore Wind Turbine Support Structures. Appendix 3-B.

Veletsos, A. S. and Wie, Y. T. 1971. Lateral and Rocking Vibration of Footings, Journal of the Soil Mechanics and Foundations Division, ASCE 95(SM9), September.

Wikipedia, The Free Encyclopedia. Bahrain World Trade Center 2010. (http://www. wikipedia.org)

Wilson, J. F. 1984. Dynamics of Offshore Structures. Wiley Interscience, New York.

Wolf, J. P. and Deeks, A. J. 2004. Foundation Vibration Analysis: A Strength of Materials Approach. Linacre House, Jordan Hill, Elsevier.

Wolf, J. P. and Meek, J. W. 1994. Cone Models for Embedded Foundation. Journal of Geotechnical Engineering 120 (1), 60-80.

Wolf, J. P. and Preisig, M. 2003. Dynamic stiffness of foundation embedded in layered half-space based on wave propagation in cones. Earthquake Engineering and Structural Dynamics 32, 1075-1098.

Yang, Y. B., Yau, J. D., and Wu, Y. S. 2004. Vehicle-Bridge Interaction Dynamics With Applications to High-Speed Railways, World Scientific, Singapore.

Zaaijer, M. B. 2005. Design Methods for Offshore Wind Turbines at Exposed Sites (OWTES). Sensitivity Analysis for Foundations of Offshore Wind Turbines, OWTES Task 4.1, OWEC Tools Task B.1-B.2, Delft University of Technology.

Zaaijer, M. B. 2002. Foundation models for the dynamic response of offshore wind turbines. Marine Renewable Energy Conference, Newcastle, UK.

APPENDIX

SUMMARY OF OFFSHORE WIND FARM PROJECTS*

Project	Country	MW	Turbine	Year	Diam.	Total Turbine Height	Hub Height	Water D. (min.)	Water D. (max.)	Distance From Shore	Reference
Vindeby	Denmark	5	11	1991	35	56	38	3	7	1.8	[1][8]
Lely	Netherlands	2	4	1994	41	60	40	2.5	5	0.8	[1]
Tunø Knob	Denmark	5	10	1995	39	65	45	4	7	5.5	[1]
Irene Vorrink	Netherlands	17	28	1996	43	72	50	2	2	0	[1]
Gotland	Sweden	3	5	1998	37	56.5	40	6	8	3	[1][4][5]
Blyth	UK	4	2	2000	62	91	60	5	9	1	[1]
Middelgrunden	Denmark	40	20	2001	72	100	64	3	6	4.7	[1]
Utgrunden	Sweden	11	7	2001	70	100	65	13	14	4.2	[1]
Yttre Stengrund	Sweden	10	5	2001	72	96	60	7	9	2	[1]
Horns Rev Phase 1	Denmark	160	80	2002	80	110	70	6	14	14	[1][6]
Frederikshavn Phase 1&2	Denmark	11	4	2003	88	123	80	1	2	3.2	[1]
Nysted Havmollepark	Denmark	166	72	2003	82	110	69	6	9	10.8	[1]
Rønland	Denmark	17	8	2003	93	120	73	0	2	0.1	[2]
Samsø	Denmark	23	10	2003	82	105	64	12	18	4	[1]
North Hoyle	UK	60	30	2004	80	107	67	7	11	7.2	[1]
Arklow Bank	Ireland	25	7	2004	50	99	74	1	35	10	[1]
Hokkaido	Japan	1	2	2004	47	71	47	13	13	0.7	[2][7]
Scroby Sands	UK	60	30	2004	80	108	68	5	10	2.3	[1]
Ems-Emdem	Germany	4.5	1	2004				3	3	0.1	[11]
Kentish Flats	UK	90	30	2005	90	115	70	5	5	8.5	[1][9]
Barrow Offshore Wind	UK	90	30	2006	90	120	75	15	20	7.5	[1]
Egmond aan Zee	Netherlands	108	36	2006	90	112	70	18	18	10	[1]

* All dimensions in meter, except "Distance From Shore" in kilometer.

[1] http://en.wikipedia.org/wiki/List_of_offshore_wind_farms
[2] http://www.renewableenergyworld.com/rea/news/article/2009/10/large-wind
[3] http://www.4coffshore.com/windfarms
[4] http://www.wind-energy-the-facts.org
[5] http://www.energyiemeteorologie.de
[6] http://www.vattenfall.com
[7] http://www.khi.co.jp/index_e.html
[8] http://www.risoe.dk
[9] http://www.kentishflats.co.uk
[10] http://www.fbbb.dk
[11]National Renewable Energy Laboratory (NREL) - September 2010

Project	Country	MW	Turbine	Year	Diam.	Total Turbine Height	Hub Height	Water D. (min.)	Water D. (max.)	Distance From Shore	Reference
Breitling	Germany	2.3	1	2006				2	2	0.5	[11]
Beatrice Demonstration	UK	10	2	2007	126	170	107	45	45	23	[1]
Burbo Offshore Wind Farm	UK	90	25	2007	107	137	84	7	12	6.4	[1]
Lillgrund	Sweden	110	48	2007	93	115	68	4	13	11.3	[1]
Kemi Ajos Phase 1&2	Finland	30	10	2008	100	138	88	1	7	2.6	[1]
Inner Dowsing	UK	97	27	2008	107	134	80	18.6	26	5	[1]
Lynn	UK	97	27	2008	107	134	80	5	10	5	[1]
Princess Amalia	Netherlands	120	60	2008	80	97	59	19	24	23	[1]
Thornton Bank	Belgium	30	6	2008	126	130	94	12	27	27	[1]
Hooksiel	Germany	5	1	2008				5	5	0.5	[11]
Brindisi	Italy	0.08	1	2008				108	108	20	[11]
Hywind	Norway	2.3	1	2009				100	100	10	[11]
Horns Rev Phase 2	Denmark	209	91	2009	93	115	68	9	17	31.7	[1]
Alpha Ventus	Germany	60	12	2009	126	155	92	28	30	56.2	[1]
Avedøre	Denmark	7.2	2	2009	120	153	93	6	8	1.4	[1][3][10]
Gasslingegrund	Sweden	30	10	2009	100	135	90	3	13	3.5	[1][3]
Rhyl Flats	UK	90	25	2009	107	134	80	6.5	12.5	8	[1]
Robin Rigg	UK	180	60	2009	90	125	80	0	20	11	[1]
Sprogø	Denmark	21	7	2009	90	115	70	6	16	10.6	[1][3]
Donghai Bridge	China	100	34	2010	90	136	91	7	7	9	[1]
BARD Offshore	Germany	400	80	2010	122	151	90	39	41	107	[1][3]
Frederikshavn	Denmark	12	6	2010							[1][3]
Gunfleet Sands	UK	172	48	2010	107	129	75	0.5	10	7	[1]
Ormonde	UK	150	30	2010	140	165	100	17	22	9.5	[1][3]
Rødsand II	Denmark	200	72	2010	93	115	68	6	12	8.8	[1]
Thanet	UK	300	100	2010	90	115	70	20	25	12	[1]
Greater Gabbard	UK	500	140	2011	130	170	105	24	34	36	[1]
Sheringham Shoal	UK	315	88	2011	104	132	80	16	22	23	[1]
Bligh Bank	Belgium	165	55	2011	90	127	72	15	37	46	[1]
Tricase	Italy	90	38	2012				33	86	20	[1]

VITA

Name: Fares Aljeeran

Address: Bayan, Block 12, Street 1, Road 1, House No. 43
Kuwait City, Kuwait

Email Address: fares355@hotmail.com

Education: B.S., Civil Engineering, Kuwait University, 1999
M.S., Ocean Engineering, Texas A&M University, 2006
Ph.D., Ocean Engineering, Texas A&M University, 2011